國 立 交 通 大 學

應用數學系數學建模與科學計算碩士班

碩士論文

動量空間時空守恆法及其應用

Momentum space conservation element and solution element method and some applications

研究生 ：黃振庭 (Zhen-Ting Huang)

指導教授: 吳宗信 博士 (Prof. Jong-Shinn Wu)

江進福 博士 (Prof. Tsin-Fu Jiang)

吳金典 博士 (Prof. Chin-Tien Wu)

西元 二零零九年七月


E S A
1896

動量空間時空守恆法及其應用

Momentum space conservation element and solution element method and some applications

國立交通大學

數學建模與科學計算研究所

碩 士 論 文

BY

Zhen-Ting Huang

B.S., National Kaohsiung University (2007)

THESIS

submitted to the National Chiao Tung University
in partial fulfillment of the
requirements for the degree of

Master of Science
in
Mathematical Modeling and Scientific Computing

May, 2009
Hsinchu, Taiwan

Table of Contents

List of Tables

List of Figures

List of Abbreviations

u, ψ	.....	wave function
a	.....	convection coefficient
E_2	.....	two-dimentional Euclidean space
SE	.....	solution element
CE	.....	conservation element
ν	.....	courant number, CFL number
μ	.....	viscosity coefficient
ξ	.....	$4\mu\triangle t/\triangle x^2$
τ	.....	parameter for courant number insensitive scheme
α	.....	weight factor for w-α scheme
ϵ	.....	convergence tolerance
F, G	.....	source term
υ	.....	parameter for Burgers's equation (related to dissipative effect)
L	.....	computational boundary
$\widehat{x}_k$	.....	grid point for non-uniform grid method
V	.....	potential
A	.....	vector potential
E	.....	electric field
q	.....	electric charge

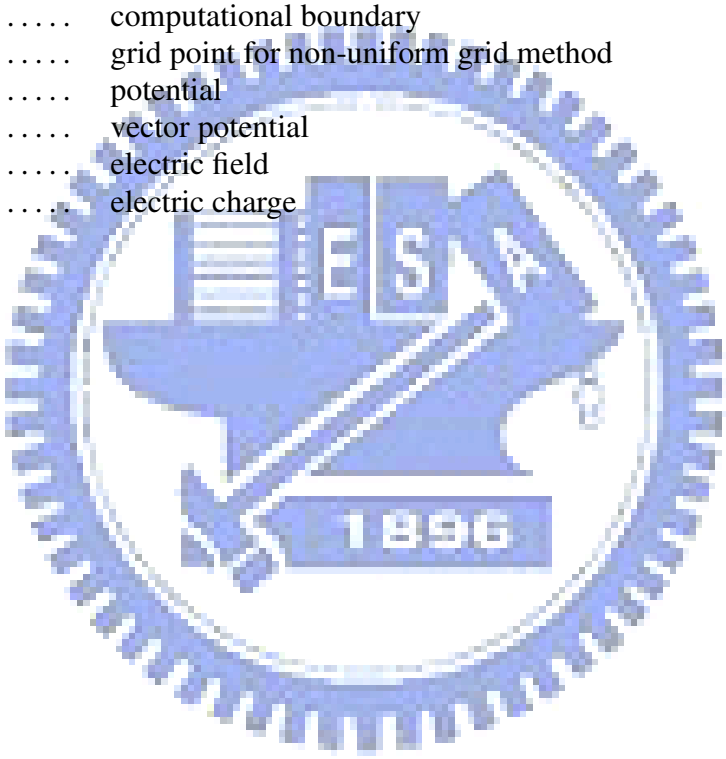

Acknowledgements

當碩士論文寫到此頁，則代表我的碩士生涯要正式落幕了，兩年的研究所時光看似漫長，實則如過眼雲煙轉瞬即逝。人生的美好不在於延續生命的永恆不滅，而在於瞬間璀璨所散發出來的繽紛光芒，雖然兩年時間匆匆而逝，但已在我的人生之中留下許多不可磨滅的奪目光采。

首先最要感謝的人是吳宗信老師，江進福老師和吳金典老師，從入學的暑假一直到畢業的暑假，整整兩年寒暑從未間斷的辛勤教導，吾以為學如逆水行舟，而老師則像是裝在舟上的電動馬達，帶我一路勇往直前奮力不倦，不僅於課業上給予指導，更教曉我做人做事的態度，如今輕舟已過萬重山，老師對我的照顧及付出，點滴在心，無限感激！在此特別一提對學生求學生涯幫助甚多的陳中壹老師，劉晉良老師和陳仁豪博士，於學生轉學和大學專題期間，對學生眾多的鼓勵和幫助，讓學生能夠累積此碩士論文所需的基本知識，學生感激在心。

於交大機械與交大物理的研究團隊中，要特別感謝楊政道同學和鄭世達學長，在物理領域中指引我許多正確的觀念，還要感謝實驗室李允民博士和李漢傑博士在學業上的啟發及教導，還有口試委員陳彥升和蘇正耀教授所提供之寶貴意見，俾使論文得以更加完善。另外，感謝同窗建興，偉任，裕昇、哲維、仁洲、昆霖等，兩年來所帶給我的歡樂，希望大家往後的日子都能夠一帆風順。

特別感謝我的家人，如不是你們一直以來的包容及支持，我也不可能有今天的小小成就。當然還要感謝這兩年對我不離不棄的伊雯大正妹，妳就像是我手心的太陽，總在我忙碌無助時，適時給予我安定的力量，支持我一路走下去，認識妳是我最大的福氣，謝謝妳！

最後，要感謝的人實在太多，如有被遺忘的朋友在此亦一併感謝，感謝大家於這兩年來對我的照顧。有些人的碩士生涯過的如黑白像片般愁雲慘淡，但我的碩士生涯用資訊豐富的高光譜影像來描述亦不為過，在此也祝福所有還在學的朋友們都能夠在求學的路上綻放出各式各樣的光芒！ 2009 年 6 月 17 日

動量空間時空守恆法及其應用

學生 ： 黃振庭　　指導教授 ： 吳宗信
：江進福, 吳金典

數學建模與科學計算研究所

中文摘要

本論文主要的研究目的為利用高解析度動量空間時空守恆法(CESE method)模擬多種一維波動方程問題並用已知的真解當作校對，最後將之應用於強場作用下單電子原子薛丁格方程式。時空守恆法為在時間和空間上均具有二階準確度的新數值方法，此時間演化的過程是一種顯式的方法。發展動量空間時空守恆法主要的動機為避免處理複雜的非反射邊界條件於座標空間和保留完整的資訊對於散射狀態。在此我們提供了完整的推演對於非反射邊界條件的處理，亦提出了各種技巧以增加解的精確度；針對非線性問題亦提出一相對的修正；最後推導出非均勻網格之動量空間時空守恆法。由數值解與解析解比較顯示，時空守恆法模擬各種情況的波方程均具有相當精確的結果。相較於座標空間的方法，於動量空間計算波方程在時間演化下仍保持完整的資訊，對於散射狀態的問題，動量空間的方法尤其適合。

Momentum space conservation element and solution element method and some applications

Zhen-Ting Huang

Institute of Mathematical Modeling and Scientific Computing

Abstract

In this thesis, the purpose of investigation is to apply high accuracy numerical scheme - the "momentum space space-time conservation element and solution element (CESE) method" to simulate several one-dimensional wave equations. Several paradigmatic wave equations are solved by the method and calibrated with known solutions. Finally, we apply the method to the problem of single atom and single-active electron Schrödinger equation with strong field. The CESE method use explicit time marching and has a second-order accuracy both in space and time. Development of the CESE method in momentum space is motivated by a goal to avoid the troubles from boundary reflection, and to preserve information completely for scattering states. In this article, we complete detail deduction for the treatment of non-reflecting boundary conditions, and the skills to improve numerical accuracy. Besides, some modifications of improving numerical accuracy needed for nonlinear problems are also introduced. In the end, we derive a non-uniform grid momentum space CESE method. Comparing the numerical results with the exact solutions for each case, we have showed that the momentum CESE method produces excellent results in each kind of wave equation. Compared to the solution in coordinate space method, this method preserves the completeness of the wave’s information during the time evolution. This is a useful feature of the momentum space method especially for the scattering state problems.

Chapter 1 Introduction

In the early 90's, the method of space-time conservation element and solution element (to be abbreviated as CESE) was developed by Chang *et al.* for solving the wave problems [1][7]. Since its inception, the CESE method shows distinguished power in solving various partial differential equations (PDEs) such as problems in computational fluid dynamics, aeroacoustics, electromagnetism and magnetohydrodynamic problems etc. [8]. The concept and methodology in this method are significantly different from those in the well-established traditional method such as the finite difference, finite element, finite volume and spectral methods. The CESE method satisfies physical concept and casts the governing equation in integral form obeyed conservation law. The time marching scheme in this method is explicit. The CESE method has many nontraditional features, such as, a unified treatment of space and time, enforced both local and global flux conservation, all the dependent variables and their derivatives are considered as individual unknowns to be solved simultaneously at each grid point, the concepts of conservation element and solution element are introduced to enforce both the local and global flux conservation without using interpolation or extrapolation, and so on.

In the CESE method, the *space coordinate* and the *time* degree of freedom are treated in a unified way. The space-time domain is discretized into solution element (SE). The non-overlap space-time cells bounded by SE are called the conservation elements (CE) as depicted in Figure 2.2. The space-time flux conservation law is enforced in each CE. Time marching scheme is then derived from the conservation law. Apply the flux conservation idea at boundary CE naturally implies the non-reflecting boundary condition (NRBC) [3]. We do not need to add filter functions and absorbing potential etc. [10] near the boundary to keep the numerical solution from contaminated by the aliased reflection generated from the boundary.

However, there is a general trouble of calculation in coordinate space. Namely, we do obtain the correct information in our model numerical region, but we lose the part of wave that flows out of our space region. In some physics problems, we also interest in the wave outside of the numerical region. For examples, in the problem of highly excited states or the photoionized electron spectrum, their wave functions both extend to very large spatial range. The coordinate space calculation becomes intractable for these problems. Theoretically, we can solve a problem in either coordinate space or momentum space representation. They are equivalent and complementary to each other in case the solution is complete. Thus, a widely diffusive wave in coordinate space is transformed to narrowly localized one in momentum space. Due to extremely large energy for a system is usually unphysical. So, only a moderate momentum region is sufficient for numerical modeling. As a result, zero Dirichlet boundary condition can be imposed in the momentum space. Solving problems in momentum space is naturally attempted.

However, the application of CESE method in momentum space has never touched to our knowledge. In this article, we aim to develop a new momentum space CESE method that reserves the power of CESE and still keeps the complete information of solution simultaneously during the time evolution. A Fourier transformation can convert momentum space solution into coordinate space representation at any time if the information in the latter is requested. The momentum space approach will then be useful for both the time-dependent systems and scattering problems. This article contains the layout of the fundamental idea of the momentum space CESE method.

The purpose of investigation is to apply high accuracy numerical scheme – the "momentum space space-time conservation element and solution element (CESE) method" to simulate several one-dimensional wave equations. Several paradigmatic wave equations are solved by the method and calibrated with known solutions. Finally, we apply the method to the problem of single atom and single-active electron Schrödinger equation with strong field [11]. For particular, we

investigate the popular research topic "strong field atomic ionization" in atomic physics, such as, above-threshold ionization (ATI) spectra. We present the results for the photoelectron spectra observed when atoms are submitted to an intense laser field, and focus our discussion of the parameters's range where conspicuous enhancements are observed in the high-energy part of the above-threshold (ATI) spectra.

Development of the CESE method in momentum space is motivated by the goal to prevent boundary reflection like method in coordinate space, and to preserve information completely for scattering states. We introduce three kind of different non-reflecting boundary conditions, and describe the complete information on how to apply it to momentum space or coordinate space method. In this article, we add an iterating process to improve numerical accuracy. For nonlinear problem, we give a modification about the convolution integral treatment which satisfies the basic idea of the solution element. In the end, we derive a non-uniform grid momentum space CESE method, and provide a method to increase accuracy about the shock wave problem. For the single-active electron systems, we introduce a simple discretization method and lead the problem into the standard eigenvalue problem. For the eigenvalue problem, we use the QZ algorithm (small size matrix) or JD method (large scale matrix) as a solver [18]. After that we obtain a pair set of eigenvalues and eigenfunctions. The reliable pseudocomplete set of momentum space eigenfunctions is then applied to the calculate of time-evolution of intense laser pulse on Ar atom. At the end of the simulation we obtaine the final state wave function. For this state, a renormalized process is introduced to confirm the normalization.

Comparing the numerical results with the exact solutions for each case, we have shown that the momentum space CESE method has excellent results in simulating the nonlinear wave function. Moreover, the momentum space CESE method also provide a reasonable numerical solution of shock wave problem. Compare to the solution methods in coordinate space, this

method preserves the complete information of the wave during the time evolution. This is a useful feature of the momentum space method especially for the scattering state problems. With the advantage of having no boundary reflection during the time evolution, the photoelectron spectra of above-threshold ionization (ATI) are elucidated. Some of which are not feasible or very difficult to solve with the coordinate space method. Generalization of the method to single-active electron systems is straightforward. In our discussion, the conspicuous enhancements appears in the high-energy part of the above-threshold (ATI) spectra, too. Because of such the basic derivation of the momentum space CESE method is realized and verified in solving many kinds of wave equation. The developed numerical method has more potential on the following works in "strong field ionization problem". The rest of this article is organized as follows: In Sec. II, we present the formulation of the CESE method for the simple wave equation. In Sec. III, we introduce the momentum space CESE method for the simple wave equation. In Sec. IV, the nonlinear Korteweg-de Vries (KdV) equation and shock wave problem are solved by momentum space CESE method. In Sec. V, the non-uniform grid momentum space CESE method is presented. And in Sec. VI, we calculate the time-dependent Schrödinger equation of single-active electron system with an intense laser field. The numerical results are given in Sec. VII and VIII. The discussion and conclusions are given in Sec. IX.

Chapter 2 Review of the CESE Method

2.1 The core scheme

The basic CESE description is followed [6]. The CESE method is enforce conservation laws locally and globally in their natural space-time unity forms and build a dissipative scheme from a non-dissipative core scheme. Computations involving a neutrally stable scheme are performed right on the edge of the instability and free of numerical dissipation. As such numerical dissipation can be controlled effectively if the deviation of a solver from its non-dissipative core scheme can be adjusted using some built-in parameters. The CESE method uses the simplest stencil. This is because the observations that direct physical interaction generally occur only among immediate neighbors and a desire to simplify boundary treatment. The CESE method evaluates the flux at an interface in a simple and consistent manner. No Riemann solvers or flux splitting techniques are used. The stability bound for each scheme is showed in the Table 2.1[1] without analysis. For more details, the references from Chang's papers are needed.

2.1.1 Convection equation

In this section, we shall introduce the 1D a-scheme described in Ref.[1]. The a-scheme has space-time staggered mesh points, two independent mesh variables and two equations per mesh point and two diagonally opposite neighboring mesh points are linked by one conservation condition and form a basic stencil.

Consider the PDE

$$\frac{\partial u}{\partial t} + a\frac{\partial u}{\partial x} = 0, \tag{2.1}$$

where the convection coefficient, $a \neq 0$, is a constant. Let x and t be the coordinate of a two

[1] The definition of $\tau_0\left(\nu^2\right)$ can see the Ref. [5].

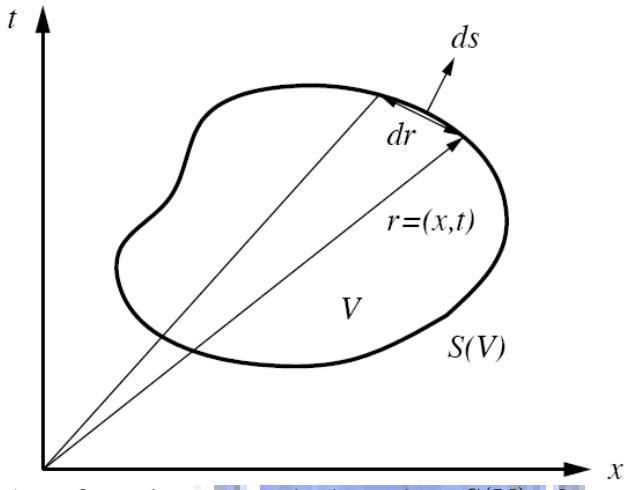

Figure 2.1: A surface element on the boundary $S(V)$ of an arbitrary space-time volume V.

dimensional Euclidean space E_2. By using Gauss divergence theorem in E_2

$$\oint_{S(V)} \overrightarrow{h} \cdot d\overrightarrow{s} = 0. \tag{2.2}$$

As depicted in Figure 2.1, $S(V)$ is the boundary of an arbitrary space-time region V in E_2, $\overrightarrow{h} = (au, u)$ is a current density vector in E_2, and the surface element $d\overrightarrow{s} = \overrightarrow{n} \cdot d\sigma$ with $d\sigma$ and $\overrightarrow{n}$ being the area and the outward unit normal vector of a surface element on $S(V)$, respectively.

As depicted in Figure 2.2, let E_2 be divided into non-overlapping rectangular regions and are referred as conservation elements (CEs). The CEs with the mesh point $(j, n) \in \Omega$ are denoted by $CE_-(j, n)$ and $CE_+(j, n)$, respectively. Each mesh point (j, n) is associated with a cross-shaped solution element.

Note that the conservation law given in Eq. (2.2) is formulated in which space and time are treated on equal footing. This unity of space and time is also a tenet in the following numerical development.

For any $(x, t) \in SE(j, n)$, $u(x, t)$, and $\overrightarrow{h}(x, t)$ are approximated by $u(x, t; j, n)$ and

$\overrightarrow{h}(x,t;j,n)$, respectively. Using the first-order Taylor's expansion of $u(x,t)$ at (x_j,t^n), we define

$$u(x,t;j,n) = u_j^n + (u_x)_j^n(x-x_j) + (u_t)_j^n(t-t^n). \tag{2.3}$$

We identify u_j^n, $(u_x)_j^n$ and $(u_t)_j^n$ with the values of u, $\partial u/\partial x$, and $\partial u/\partial t$ at (x_j,t^n), respectively. Not that u_j^n, $(u_x)_j^n$ and $(u_t)_j^n$ are constants in $SE(j,n)$. Requiring that $u=(x,t;j,n)$ satisfies Eq. (2.1) within $SE(j,n)$, one has

$$(u_t)_j^n = -a(u_x)_j^n. \tag{2.4}$$

Substitution Eq. (2.4) into Eq. (2.3), one has

$$u(x,t;j,n) = u_j^n + [(x-x_j) - a(t-t^n)]\,(u_x)_j^n. \tag{2.5}$$

Note that the expansion coefficients u_j^n and $(u_x)_j^n$ in Eq. (2.5) are treated as independent variables. In addition, $\overrightarrow{h}$ is approximated by

$$\overrightarrow{h}(x,t;j,n) = (au(x,t;j,n), u(x,t;j,n)). \tag{2.6}$$

With the approximation, the total flux leaving the boundary of $CE_{\pm}(j,n)$ is

$$F_{\pm}(j,n) = \oint_{S(CE_{\pm}(j,n))} \overrightarrow{h}\cdot d\overrightarrow{s} = 0,\ (j,n)\in\Omega. \tag{2.7}$$

As depicted in Figure 2.2 for CE_-, the outward unit normal vectors $\overrightarrow{n}$ at $\overline{AD}$, $\overline{AE}$, $\overline{BE}$ and $\overline{BD}$ are $(1,0)$, $(0,1)$, $(-1,0)$ and $(0,-1)$, respectively; and for CE_+, the outward unit normal vectors $\overrightarrow{n}$ at $\overline{AD}$, $\overline{AF}$, $\overline{CF}$ and $\overline{CD}$ are $(-1,0)$, $(0,1)$, $(1,0)$ and $(0,-1)$, respectively. By using Eqns. (2.5) , and (2.6), it can be shown that Eq. (2.7) is equivalent to

$$(1\mp\nu)\left[u\pm(1\pm\nu)u_{\overline{x}}\right]_j^n = (1\mp\nu)\left[u\mp(1\pm\nu)u_{\overline{x}}\right]_{j\pm\frac{1}{2}}^{n-\frac{1}{2}}, \tag{2.8}$$

where $\nu\equiv a\triangle t/\triangle x$ and $(u_{\overline{x}})_j^n \equiv \frac{\triangle x}{4}(u_x)_j^n$.

Choose $1-\nu\neq 0$ and $1+\nu\neq 0$. Eq. (2.8) reduce to

$$\left[u\pm(1\pm\nu)u_{\overline{x}}\right]_j^n = \left[u\mp(1\pm\nu)u_{\overline{x}}\right]_{j\pm\frac{1}{2}}^{n-\frac{1}{2}}. \tag{2.9}$$

By using Eq. (2.9), u_j^n and $(u_{\overline{x}})_j^n$ can be solved in term of $u_{j\pm\frac{1}{2}}^{n-\frac{1}{2}}$ and $(u_{\overline{x}})_{j\pm\frac{1}{2}}^{n-\frac{1}{2}}$. The time-marching

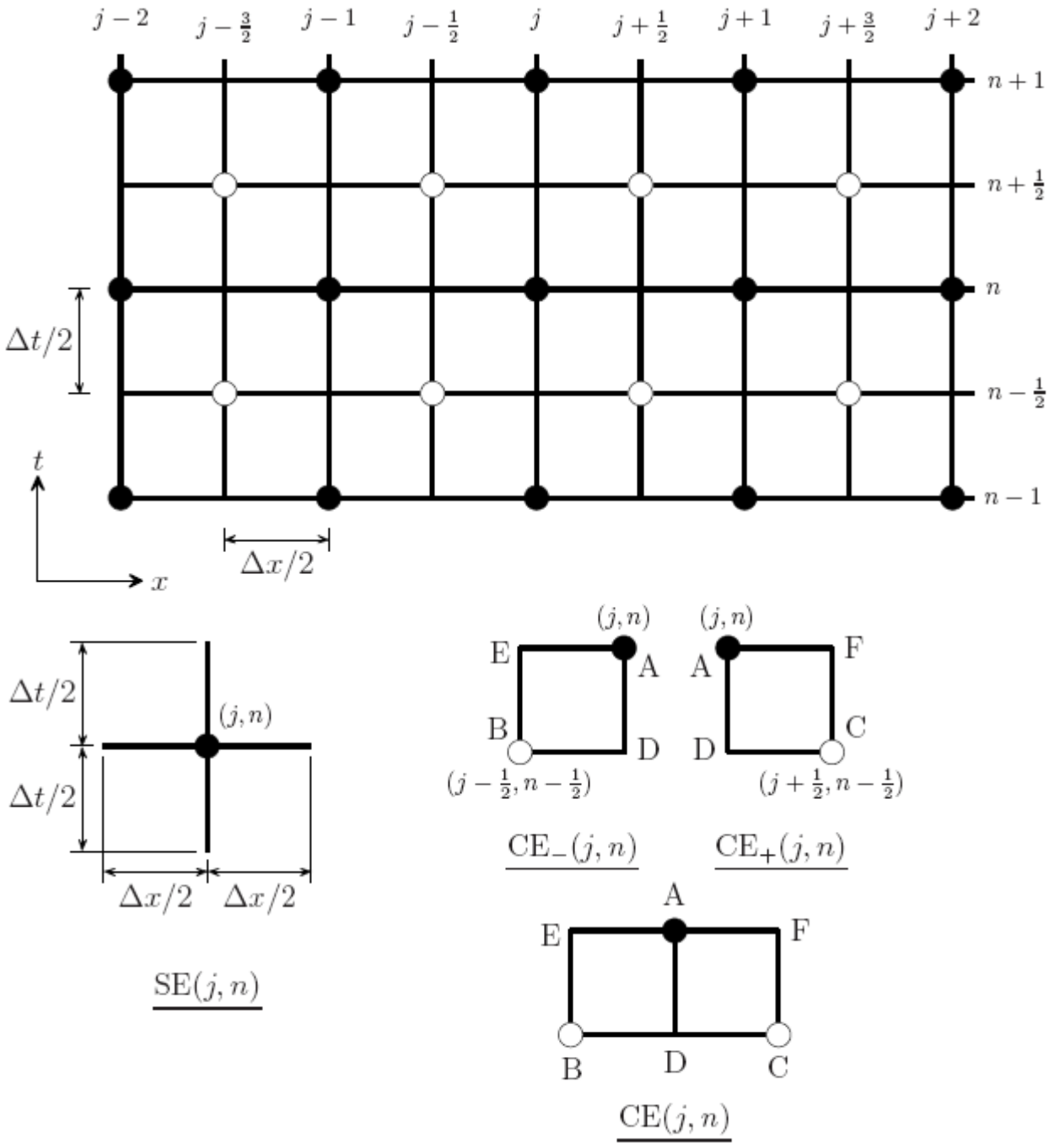

Figure 2.2: Definitions of the space-time staggered mesh, CE and SE in E_2.

is then arrived by explicit iterations.

$$\begin{cases} u_j^n = \frac{1}{2}\left\{(1-\nu)\left[u-(1+\nu)u_{\overline{x}}\right]_{j+\frac{1}{2}}^{n-\frac{1}{2}} + (1+\nu)\left[u+(1-\nu)u_{\overline{x}}\right]_{j-\frac{1}{2}}^{n-\frac{1}{2}}\right\}, \\ (u_{\overline{x}}^a)_j^n \equiv (u_{\overline{x}})_j^n = \frac{1}{2}\left\{\left[u-(1+\nu)u_{\overline{x}}\right]_{j+\frac{1}{2}}^{n-\frac{1}{2}} - \left[u+(1-\nu)u_{\overline{x}}\right]_{j-\frac{1}{2}}^{n-\frac{1}{2}}\right\}. \end{cases} \tag{2.10}$$

The matrix forms of the a-scheme: Let

$$\begin{aligned} \overrightarrow{q}(j,n) &\equiv \begin{pmatrix} u_j^n \\ (u_{\overline{x}})_j^n \end{pmatrix}, \ (j,n) \in \Omega, \\ Q_+(\nu) &\equiv \frac{1}{2}\begin{pmatrix} 1-\nu & -(1-\nu^2) \\ 1 & -(1+\nu) \end{pmatrix}, \\ Q_-(\nu) &\equiv \frac{1}{2}\begin{pmatrix} 1+\nu & 1-\nu^2 \\ -1 & -(1-\nu) \end{pmatrix}. \end{aligned} \tag{2.11}$$

Then the forward marching forms of the a-scheme can be cast into the matrix forms

$$\overrightarrow{q}(j,n) = Q_+(\nu)\overrightarrow{q}(j+\frac{1}{2},n-\frac{1}{2}) + Q_-(\nu)\overrightarrow{q}(j-\frac{1}{2},n-\frac{1}{2}). \tag{2.12}$$

2.1.2 Convection-diffusion equation

Refer to Ref.[2], consider the dimensionless form of the one-dimensional convection-diffusion equation

$$\frac{\partial u}{\partial t} + a\frac{\partial u}{\partial x} - \mu\frac{\partial^2 u}{\partial x^2} = 0, \tag{2.13}$$

where the wave velocity a, and the viscosity coefficient μ are constants. By using Gauss divergence theorem in E_2,

$$\oint_{S(V)} \overrightarrow{h}\cdot d\overrightarrow{s} = 0,$$

where $\overrightarrow{h} = (au - \mu u_x, u)$.

Let $u = u(x,t;j,n)$ be defined by Eq. (2.3), it satisfies Eq. (2.13). Within $SE(j,n)$, one has

$$(u_t)_j^n = -a(u_x)_j^n. \tag{2.14}$$

Substituting Eq. (2.14) into Eq. (2.3), one has

$$u(x,t;j,n) = u_j^n + \left[(x-x_j) - a(t-t^n)\right](u_x)_j^n. \tag{2.15}$$

In addition, we have the approximation

$$\overrightarrow{h}(x,t;j,n) = (au(x,t;j,n) - \mu u_x(x,t;j,n), u(x,t;j,n)). \tag{2.16}$$

The approximation is defined by Eq. (2.7), the total flux which leaves the boundary of

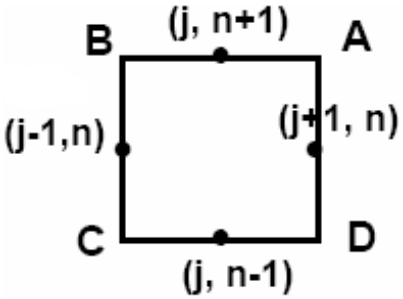

Figure 2.3: Conservation element for the leapfrog scheme.

$CE_{\pm}(j,n)$ also can be used here. And we obtain

$$\frac{4}{\triangle x^2}F_{\pm}(j,n) = \pm\frac{1}{2}\left[(1-\nu^2+\xi)(u_x)_j^n + (1-\nu^2-\xi)(u_x)_{j\pm\frac{1}{2}}^{n-\frac{1}{2}}\right] + \frac{2(1\mp\nu)}{\triangle x}\left(u_j^n - u_{j\pm\frac{1}{2}}^{n-\frac{1}{2}}\right) = 0, \tag{2.17}$$

where $\nu = a\triangle t/\triangle x$ and $\xi = 4\mu\triangle t/\triangle x^2$.

By Eq. (2.17), u_j^n and $(u_x)_j^n$ can be solved in term of $(u)_{j\pm\frac{1}{2}}^{n-\frac{1}{2}}$ and $(u_x)_{j\pm\frac{1}{2}}^{n-\frac{1}{2}}$ if $1-\nu^2+\xi \neq 0$. The time-marching scheme is then arrived by explicit iterations. Here we let $(u_{\overline{x}})_j^n \equiv \frac{\triangle x}{4}(u_x)_j^n$, $\overrightarrow{q}(j,n) \equiv \begin{pmatrix} u_j^n \\ (u_{\overline{x}})_j^n \end{pmatrix}$ for all $(j,n) \in \Omega$; $Q_+(\nu) \equiv \frac{1}{2}\begin{pmatrix} 1-\nu & -(1-\nu^2-\xi) \\ \frac{1-\nu^2}{1-\nu^2+\xi} & -\frac{(1+\nu)(1-\nu^2-\xi)}{1-\nu^2+\xi} \end{pmatrix}$ and $Q_-(\nu) \equiv \frac{1}{2}\begin{pmatrix} 1+\nu & 1-\nu^2-\xi \\ -\frac{(1-\nu^2)}{1-\nu^2+\xi} & -\frac{(1-\nu)(1-\nu^2-\xi)}{1-\nu^2+\xi} \end{pmatrix}$. Then it can be cast into the matrix forms like Eq. (2.12). The a-μ scheme is formed, and it is easy to see it becomes a-scheme if $\mu = 0$.

2.1.3 Comments on Leapfrog scheme

The leapfrog scheme

$$\frac{u_j^{n+1} - u_j^{n-1}}{2\triangle t} + \frac{u_{j+1}^n - u_{j-1}^n}{2\triangle x} = 0, \ (j,n+1) \in \Omega. \tag{2.18}$$

can also be cast into the conservation form

$$\oint_{S(FV(j,n+1))} \overrightarrow{h} \cdot d\overrightarrow{s} = 0, \ (j,n+1) \in \Omega. \tag{2.19}$$

where $FV(j,n+1)$ is the region $ABCD$ depicted in Figure 2.3. The average flux vectors $\overrightarrow{h}$ at $\overline{AB}$, $\overline{BC}$, $\overline{CD}$ and $\overline{DA}$ are taking to be $\left(au_j^{n+1}, u_j^{n+1}\right)$, $\left(au_{j-1}^n, u_{j-1}^n\right)$, $\left(au_j^{n-1}, u_j^{n-1}\right)$ and $\left(au_{j+1}^n, u_{j+1}^n\right)$, respectively.

The leapfrog scheme shares with the a-scheme three key nontraditional features, i.e., they both are explicit two-way marching schemes, have space-time staggered stencils and their interface fluxes can be evaluated without using any interpolation or extrapolation technique. The CESE a-scheme can be derived into the leapfrog scheme, but not vice a versa.

2.2 Dissipative extension of the core scheme

For these extensions, instead of the conservation conditions over $CE_{\pm}(j,n)$, $(j,n) \in \Omega$, the less stringent conservation conditions

$$\oint_{S(CE(j,n))} \overrightarrow{h} \cdot d\overrightarrow{s} = 0, \ (j,n) \in \Omega \tag{2.20}$$

are imposed. The local conservation condition Eq. (2.20) leads to a global conservation condition. Because Eq. (2.20) $\Leftrightarrow$

$$u_j^n = \frac{1}{2}\left\{(1-\nu)\left[u-(1+\nu)u_{\overline{x}}\right]_{j+\frac{1}{2}}^{n-\frac{1}{2}} + (1+\nu)\left[u+(1-\nu)u_{\overline{x}}\right]_{j-\frac{1}{2}}^{n-\frac{1}{2}}\right\}. \tag{2.21}$$

Eq. (2.21) is shared by the a-scheme and any of its dissipative extensions. In other words, a dissipative extension differs form a-scheme only in how $(u_{\overline{x}})_j^n$ is evaluated.

To proceed, consider any $(j,n) \in \Omega$. Then $\left(j_{\pm 1/2}, n-1/2\right) \in \Omega$. Let

$$u'^n_{j\pm\frac{1}{2}} \equiv u_{j\pm\frac{1}{2}}^{n-\frac{1}{2}} + \left(\frac{\triangle t}{2}\right)(u_t)_{j\pm\frac{1}{2}}^{n-\frac{1}{2}}. \tag{2.22}$$

With the aid of $(u_{\overline{x}})_j^n \equiv \frac{\triangle x}{4}(u_x)_j^n$ and the fact that the Courant number $\nu \equiv a\triangle t/\triangle x$, a substitution of the relation $(u_t)_j^n = -a(u_x)_j^n$ into Eq. (2.22) results in

$$u'^n_{j\pm\frac{1}{2}} \equiv \left(u - 2\nu u_{\overline{x}}\right)_{j\pm\frac{1}{2}}^{n-\frac{1}{2}}. \tag{2.23}$$

Note that, to simplify notation, in the above and hereafter we adopt a convention that can be explained using the expression on the right side of Eq. (2.23) as an example, i.e.,

$$u'^n_{j\pm\frac{1}{2}} \equiv u_{j\pm\frac{1}{2}}^n - 2\nu\left(u_{\overline{x}}\right)_{j\pm\frac{1}{2}}^{n-\frac{1}{2}}. \tag{2.24}$$

According to Eq. (2.24), $u'^n_{j\pm\frac{1}{2}}$ can be interpreted as a frst-order Taylor's approximation of u at

Table 2.1: The stability bound for each scheme.

a-scheme	c-scheme	c-τ scheme	a-μ scheme	w-α scheme
$\|\nu\| < 1$	$\|\nu\| < 1$	$\nu^2 \leq 1, \tau \geq \tau_0(\nu^2)$	$\nu^2 \leq 1$	$\|\nu\| < 1, \alpha \geq 0$

$\left(j \pm \frac{1}{2}, n\right)$. Thus

$$(u_{\overline{x}}^c)_j^n \equiv \frac{\triangle x}{4}\left(\frac{u'^n_{j+\frac{1}{2}} - u'^n_{j-\frac{1}{2}}}{\triangle x}\right) \tag{2.25}$$

is a central-difference approximation of $\partial u/\partial \overline{x}$ at (j, n). Note that: (i) the superscript "c" is used to remind the reader of the central-difference nature of the term $(u_{\overline{x}}^c)_j^n$; and (ii) by using Eqs. (2.23) and (2.25), it becomes

$$(u_{\overline{x}}^c)_j^n = \frac{1}{4}\left[(u - 2\nu u_{\overline{x}})_{j+\frac{1}{2}}^{n-\frac{1}{2}} - (u - 2\nu u_{\overline{x}})_{j-\frac{1}{2}}^{n-\frac{1}{2}}\right]. \tag{2.26}$$

The Eq. (2.21) and Eq. (2.26) forms the c-scheme.

2.3 The Courant Number Insensitive scheme

2.3.1 Advantages and Disadvantages of the a-scheme and c-scheme

The advantages of the a-scheme: (i) It is nondissipative. (ii) Vary accurate when $\nu \to 0$.; The disadvantages: (i) Due to its nondissipative nature, nonlinear extensions generally are unstable. (ii) When $|\nu| \to 1$, the short-wavelength errors will not die out rapidly and appear as persistent numerical wiggles. (iii) Comparing with the c-scheme, it costs more times to implement.

The advantages of the c-scheme: (i) Due to its dissipative nature, nonlinear extensions tend to be more stable. (ii) When $|\nu| \to 1$, it is vary accurate. The short wavelength errors die out rapidly. (iii) It much more superior than a-scheme in terms of ease of implementation.; The disadvantages: (i) it is very dissipative when $\nu \to 0$.

2.3.2 Courant Number Insensitive scheme

The basic idea of the courant number insensitive scheme follows the Chang's papers: [4][5]. In this section, the ideal solvers of Eq. (2.1) will be constructed. It is constructed such that they possess all the advantages but none of the disadvantages of the a-scheme and the c-scheme.

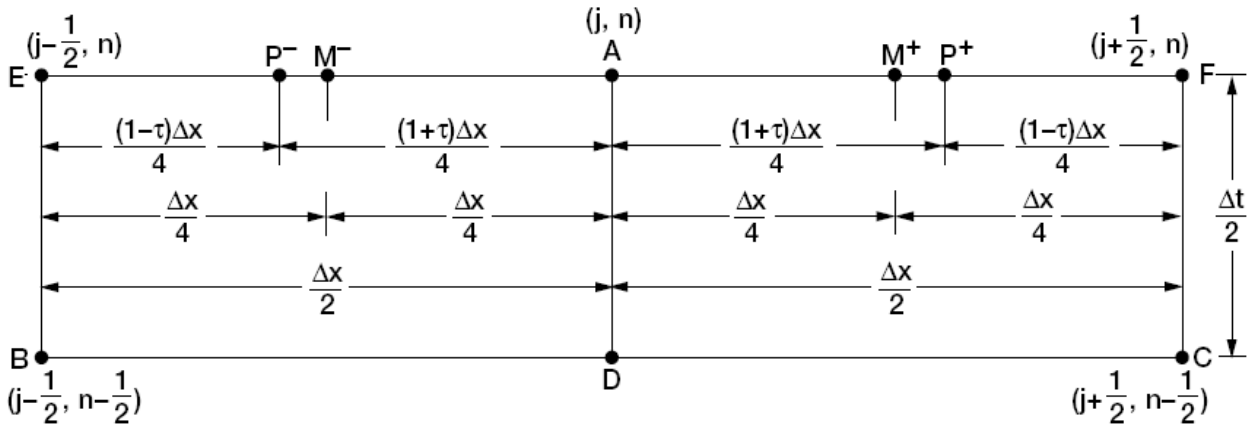

Figure 2.4: Definition of points $P^{\pm}$ and $M^{\pm}$.

Specifically, each solver is formed by Eq. (2.21) and a new equation in which $(u_{\overline{x}})_j^n$ is evaluated using a simple central-differencing procedure similar to that used to obtain $(u_{\overline{x}}^c)_j^n$ and so obtained is identical to (i) $(u_{\overline{x}}^c)_j^n$ when $|\nu| \to 1$, (ii) $(u_{\overline{x}}^a)_j^n$ when $\nu \to 0$. As such, each solver is comparable to the c-scheme in ease of implementation, becomes the c-scheme when $|\nu| \to 1$ and becomes the a-scheme when $\nu \to 0$. As a preliminary, we shall show that $(u_{\overline{x}}^a)_j^n$ can also be cast into a central-difference form when $\nu = 0$.

To proceed, note that by assumption $a \neq 0$. Thus $\nu = 0$ if and only if $\triangle t = 0$. Because $\left|\overline{EB}\right| = \left|\overline{AD}\right| = \left|\overline{FC}\right| = 0$ (see Figure. 2.4) when $\triangle t = 0$, the two conservation condition given in Eq. (2.9) becomes

$$[u \pm u_{\overline{x}}]_j^n = [u \mp u_{\overline{x}}]_{j\pm\frac{1}{2}}^{n-\frac{1}{2}}. \tag{2.27}$$

An immediate result of Eq. (2.27) is

$$(u_{\overline{x}})_j^n = \frac{1}{2}\left\{[u - u_{\overline{x}}]_{j+\frac{1}{2}}^{n-\frac{1}{2}} - [u + u_{\overline{x}}]_{j-\frac{1}{2}}^{n-\frac{1}{2}}\right\}. \tag{2.28}$$

Moreover, $[u - u_{\overline{x}}]_{j+\frac{1}{2}}^{n-\frac{1}{2}}$ and $[u + u_{\overline{x}}]_{j-\frac{1}{2}}^{n-\frac{1}{2}}$, respectively, represent approximations of u at the midpoints of $\overline{AE}$ and $\overline{AF}$; and the distance between these two midpoint is $\triangle x/2$. Thus, at $\nu = 0$, $(u_{\overline{x}}^a)_j^n$ is a central-difference approximation of $u_{\overline{x}}$ at (j, n).

Let M^+ and M^- be the midpoints of $\overline{AF}$ and $\overline{AE}$ respectively.(see Figure 2.4) Also when $\tau > 0$, P^+ is to the right of M^+ and P^- is to the left of M^-. Let

$$u'(P^{\pm}) \equiv \left[u + (\frac{\triangle t}{2})u_t \mp (1-\tau)(\frac{\triangle x}{4})u_x\right]_{j\pm\frac{1}{2}}^{n-\frac{1}{2}}. \tag{2.29}$$

By using $(u_{\overline{x}})_j^n \equiv \frac{\triangle x}{4}(u_x)_j^n$ and $(u_t)_j^n = -a(u_x)_j^n$, one has

$$u'(P^{\pm}) \equiv \left[u \mp (1 \pm 2\nu - \tau)u_{\overline{x}}\right]_{j\pm\frac{1}{2}}^{n-\frac{1}{2}}. \tag{2.30}$$

Because point A is the midpoint of $\overline{EF}$, and $\left|\overline{P^+P^-}\right| = (1+\tau)\frac{\triangle x}{2}$,

$$(\widehat{u}_{\overline{x}})_j^n \equiv \left(\frac{u'(P^+) - u'(P^-)}{2(1+\tau)}\right), \ (\tau \neq -1), \tag{2.31}$$

represents a central-difference analogue of $u_{\overline{x}}$ at (j,n). Thus a solver for Eq. (2.1) (the c-τ scheme) can be formed by Eq. (2.21) and

$$(u_{\overline{x}})_j^n = (\widehat{u}_{\overline{x}})_j^n \tag{2.32}$$

There has a sub-scheme of c-τ scheme, so called c-τ^* scheme. This scheme is just let $\tau = f(\nu)$, i.e., it means the number of τ is dependent of the number of ν. The question of finding the optimal function f is on developing. It's still an open problem.

2.4 The Wiggle-suppressing scheme

If discontinuities are present in a numerical solution, any scheme such as the c-scheme is not equipped to suppress numerical wiggles that generally appear near these discontinuities. To overcome this problem, we introduce a weighted-average method. It is the final scheme we use in the realistic computation.

To proceed, let

$$\begin{aligned}(\widehat{u}_{\overline{x}+})_j^n &\equiv \frac{\triangle x}{4}\left(\frac{u'(P^+) - u_j^n}{(1+\tau)\triangle x/4}\right), \text{ and} \\ (\widehat{u}_{\overline{x}-})_j^n &\equiv \frac{\triangle x}{4}\left(\frac{u_j^n - u'(P^-)}{(1+\tau)\triangle x/4}\right).\end{aligned} \tag{2.33}$$

Because $\left|\overline{AP^-}\right| = \left|\overline{AP^+}\right| = (1+\tau)\triangle x/4$ (see Figure 2.4), it is easy to see that $(\widehat{u}_{\overline{x}+})_j^n$ and $(\widehat{u}_{\overline{x}+})_j^n$ are two one-sided difference approximation of $u_{\overline{x}}$ at the mesh point (j,n) with one being

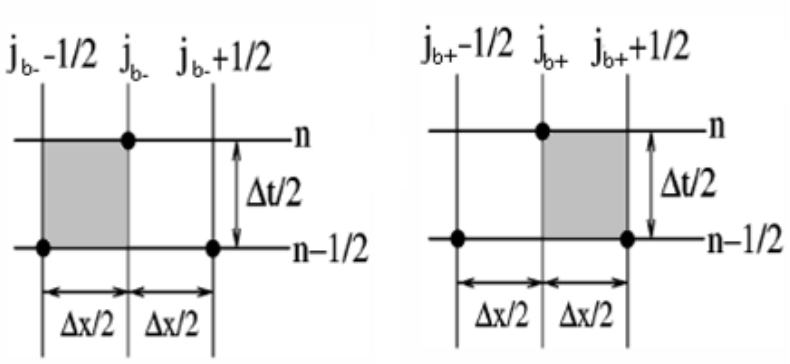

Figure 2.5: Ghost cells for the boundary.

evaluated from the left and another from the right. The new extension is formed by Eq. (2.21) and

$$(u_{\overline{x}})_j^n = \left(\omega_-^{'}\right)_j^n (\widehat{u}_{\overline{x}+})_j^n + \left(\omega_+^{'}\right)_j^n (\widehat{u}_{\overline{x}-})_j^n \tag{2.34}$$

or

$$(u_{\overline{x}})_j^n = (\widetilde{\omega}_-)_j^n (\widehat{u}_{\overline{x}+})_j^n + (\widetilde{\omega}_+)_j^n (\widehat{u}_{\overline{x}-})_j^n. \tag{2.35}$$

The definition of weight factor $\omega_\pm^{'}$ and $\widetilde{\omega}_\pm$ is described in the appendix A.

2.5 Boundary treatment

At the boundary, we add the ghost cell. As depicted in Figure 2.5, we let

$$\begin{aligned} u_{j_{b+}+\frac{1}{2}}^{n-\frac{1}{2}} &= u_{j_{b+}-\frac{1}{2}}^{n-\frac{1}{2}};\ u_{\overline{x}j_{b+}+\frac{1}{2}}^{n-\frac{1}{2}} = 0 \text{ or } u_{\overline{x}j_{b+}+\frac{1}{2}}^{n-\frac{1}{2}} = u_{\overline{x}j_{b+}-\frac{1}{2}}^{n-\frac{1}{2}}, \\ u_{j_{b-}-\frac{1}{2}}^{n-\frac{1}{2}} &= u_{j_{b-}+\frac{1}{2}}^{n-\frac{1}{2}};\ u_{\overline{x}j_{b-}-\frac{1}{2}}^{n-\frac{1}{2}} = 0 \text{ or } u_{\overline{x}j_{b-}-\frac{1}{2}}^{n-\frac{1}{2}} = u_{\overline{x}j_{b-}+\frac{1}{2}}^{n-\frac{1}{2}}. \end{aligned} \tag{2.36}$$

, then there are CE_+ (with the ghost cell) and CE_- for $u_{j_{b+}}^n$ and $u_{\overline{x}j_{b+}}^n$ ($u_{j_{b-}}^n$ and $u_{\overline{x}j_{b-}}^n$).

For the high-order scheme, the above method is not good enough. Because of the higher-derivative term is always zero. We introduce a new approach for non-reflecting boundary condition (NRBC) as

$$\begin{aligned} u_{j_{b+}+\frac{1}{2}}^{n-\frac{1}{2}} &= u_{j_{b+}-\frac{1}{2}}^{n-\frac{1}{2}} + \triangle x u_{\overline{x}j_{b+}-\frac{1}{2}}^{n-\frac{1}{2}}, \\ u_{j_{b-}-\frac{1}{2}}^{n-\frac{1}{2}} &= u_{j_{b-}+\frac{1}{2}}^{n-\frac{1}{2}} + \triangle x u_{\overline{x}j_{b-}+\frac{1}{2}}^{n-\frac{1}{2}}. \end{aligned} \tag{2.37}$$

, instead.

Chapter 3 Momentum Space CESE Method

3.1 The core scheme of the momentum space CESE method

The momentum space CESE method is developed to conquer the problems of wave propagation out of the boundary and ease the boundary treatment etc.. When the wave progresses out of the boundary, no matter how boundary condition we use the information of the wave has lost. To treat the scattering problem the momentum space CESE method shows its useful capability. The original CESE method is second-order accuracy method. It approximates the numerical solution by second-order Taylor expansion. The higher derivative term is truncated as an error. It shows that the convection-diffusion equation Eq. (2.13) has loss its' capability of accuracy when the viscosity coefficient is large. However, it is natural problem of the second order scheme. Because of the higher derivative term is truncated, the accuracy is only to first derivative term. The higher-order CESE method is to be developed for more diffusive cases in the future. In this section, we propose the momentum space CESE method. The higher derivative term is transformed to the source term. The second order scheme is enough to keep the accuracy if the source term is accurate enough. The momentum space CESE method uses the iterating process to keep the source term accuracy. For the explicit scheme, it has to keep the stability, i.e. the $\triangle t$ can not too large. It is time consuming for the explicit scheme. The iterating process added in each time step. Even if the iterations is few, it is still time consuming. But it is not a big problem for us, because of the space domain is smaller than the coordinate space method. For the quantum problem we describe in chapter 6, the domain for the momentum space CESE method is only $[-5, 5]$. For coordinate space method, the box size is must ≈ 3300 (see Ref.[13]). The total computing time of the time evolution is comparable for the coordinate space method, even it is shorter than it. However the momentum space CESE method is now a useful scheme to treat the

large diffusive problems. But for the future the higher-order CESE method will be developed. The higher-order CESE method can be easily extended to the momentum space CESE method. The basic momentum space CESE method is proposed to see its capability to keep accuracy even the equation is more diffusive.

3.1.1 Convection equation

Eq. (2.1) can be transformed into

$$\frac{\partial \widetilde{u}}{\partial t} + iap\widetilde{u} = 0, \tag{3.1}$$

by making the Fourier transformation, the system has the coordinate and the momentum representation alternatively:

$$\begin{aligned} u(x,t) &= \int \widetilde{u}(p,t)e^{ipx}dp, \\ \widetilde{u}(p,t) &= \frac{1}{2\pi}\int u(x,t)e^{-ipx}dx. \end{aligned}$$

For simplicity, we just use the same symbol u instead of $\widetilde{u}$. The Eq. (3.1) becomes $\partial u/\partial t + iapu = 0$. This is simply an ordinary differential equation. Its analytic solution is straightforward. With initial condition $u(p, t = 0)$, the solution at any time is $u(p,t) = u(p,t=0)e^{-ipat}$. Obviously, the amplitude of the solution $u(p,t)$ is stationary at any time in the momentum space. Though the equation and its solution in momentum space are rather simple, they serve as the calibration example for the momentum space CESE method. The Eq. (3.1) equivalently be written as

$$\nabla \cdot (0, u) = -iapu, \tag{3.2}$$

where the operator $\nabla = (\partial/\partial p, \partial/\partial t)$. Consider p and t as the coordinates of a two-dimensional Euclidean space E_2. The conservation laws becomes

$$\oint_{S(V)} \overrightarrow{h} \cdot d\overrightarrow{s} = -ia\int_V pud\tau, \tag{3.3}$$

where $\overrightarrow{h} = (0, u)$, $d\tau = dpdt$ and $-iapu$ is the net flux per unit volume.

Let E_2 be divided into non-overlapping rectangular regions referred to as conservation elements CEs. The CEs with the mesh point $(j, n) \in \Omega$ are denoted by $CE_-(j, n)$ and $CE_+(j, n)$,

respectively. Let $SE(j,n)$ be the rhombus shaped area DEGF depicted in Figure 3.1. The function value at the the center of $CE_{\pm}$ can be approximated by $u_{j\pm\frac{1}{2}}^{n-\frac{1}{2}}$, $(u_p)_{j\pm\frac{1}{2}}^{n-\frac{1}{2}}$ and $(u_t)_{j\pm\frac{1}{2}}^{n-\frac{1}{2}}$.

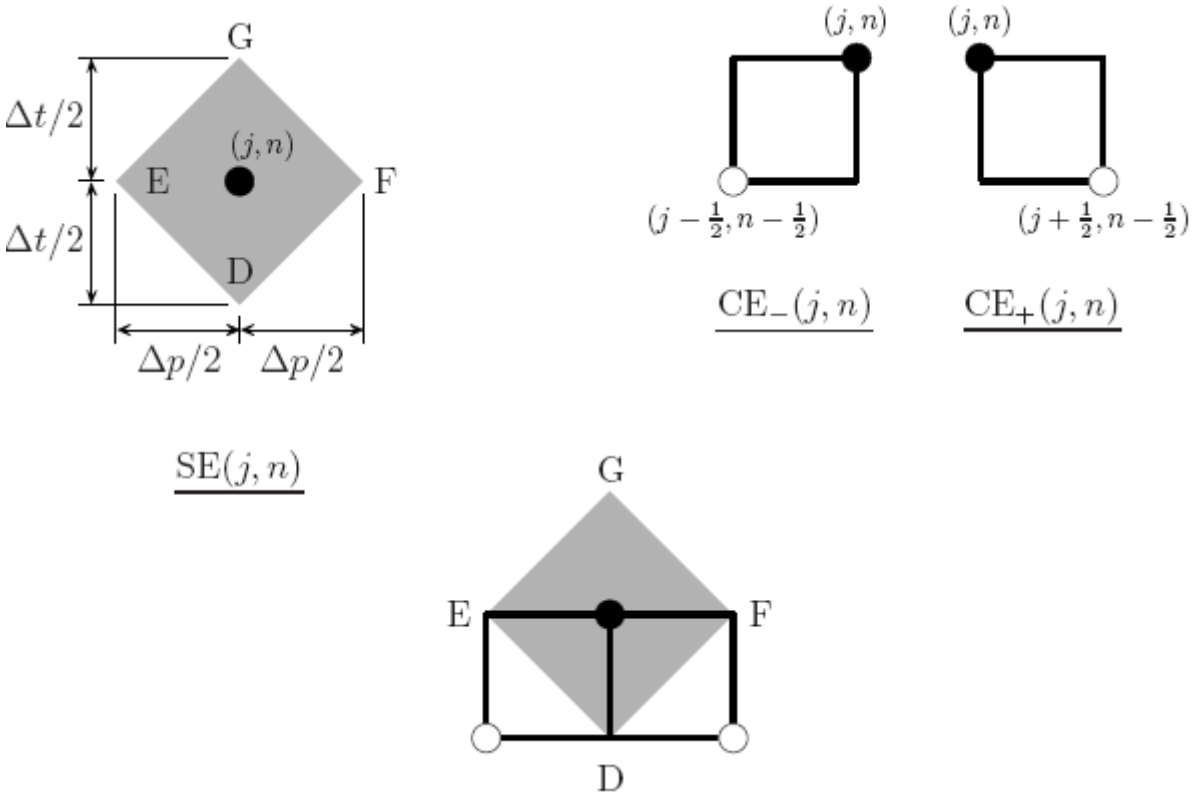

Definitions of CE and SE in E_2.

For any $(p,t) \in SE(j,n)$, $u(p,t)$ and $\overrightarrow{h}(p,t)$ are approximated by $u(p,t;j,n)$ and $\overrightarrow{h}(p,t;j,n)$, respectively. We define

$$u(p,t;j,n) = u_j^n + (u_p)_j^n(p-p_j) + (u_t)_j^n(t-t^n), \tag{3.4}$$

where (p_j,t^n) is the coordinate of the mesh point (j,n).

Note that u_j^n, $(u_p)_j^n$ and $(u_t)_j^n$ are constants in $SE(j,n)$. We also have

$$\overrightarrow{h}(p,t;j,n) = (0,u(x,t;j,n)). \tag{3.5}$$

Requiring that $u = u(p,t;j,n)$ satisfies Eq. (3.1) within $SE(j,n)$, one has

$$(u_t)_j^n = -iap_j u_j^n. \tag{3.6}$$

The approximation of the total flux leaving the boundary of $CE_{\pm}(j,n)$ is

$$F_{\pm}(j,n) = \oint_{S(CE_{\pm}(j,n))} \overrightarrow{h} \cdot d\overrightarrow{s} = -ia \int_{CE_{\pm}(j,n)} pud\tau. \tag{3.7}$$

By Eqs. (3.5) and (3.7), the total flux leaving $CE_{\pm}(j,n)$ can be derived as

$$F_{\pm}(j,n) = \frac{\triangle p}{2}\left\{u_j^n \pm (u_{\overline{p}})_j^n - \left[(u)_{j\pm\frac{1}{2}}^{n-\frac{1}{2}} \mp (u_{\overline{p}})_{j\pm\frac{1}{2}}^{n-\frac{1}{2}}\right]\right\} = -ip_{j\pm\frac{1}{4}}\left[(u)_{j\pm\frac{1}{2}}^{n-\frac{1}{2}} \mp (u_{\overline{p}})_{j\pm\frac{1}{2}}^{n-\frac{1}{2}} + \frac{1}{4}(u_t)_{j\pm\frac{1}{2}}^{n-\frac{1}{2}}\right]\frac{\triangle p}{2}\frac{\triangle t}{2}, \tag{3.8}$$

where we use Taylor expansion to estimate the function value at the center of $CE_{\pm}$ and we also designate $u_{\overline{p}} = \frac{\triangle p}{4}u_p$. In this section, the value of $(u_t)_j^n$ is easy to solve. Using the transform in Eq. (3.6), we can easily obtain the value of $(u_t)_j^n$. So the iterating process is not necessary. Here we just show that the iterating process also works in linear cases. For the following nonlinear cases the value of $(u_t)_j^n$ has convolution integral with unknown value. It is not easy to solve like the simple case here. In order to prepare for nonlinear situation (in chapter 4). With the aid of Eqs. (3.6) and (3.8), u_j^n and $(u_{\overline{p}})_j^n$ can be solved in terms of $(u)_{j\pm\frac{1}{2}}^{n-\frac{1}{2}}$ and $(u_{\overline{p}})_{j\pm\frac{1}{2}}^{n-\frac{1}{2}}$, and for further iterations,

$$u_{j,\ell}^n \pm (u_{\overline{p}})_{j,\ell}^n - \left[(u)_{j\pm\frac{1}{2}}^{n-\frac{1}{2}} \mp (u_{\overline{p}})_{j\pm\frac{1}{2}}^{n-\frac{1}{2}}\right] = -ip_{j\pm\frac{1}{4}}\left[u_{j,\ell-1}^{n-\frac{1}{2}} \mp (u_{\overline{p}})_{j,\ell-1}^{n-\frac{1}{2}}\right]\frac{\triangle t}{2}. \tag{3.9}$$

We can check the convergence of u_j^n. Eq. (3.9) can also be derived from Eq. (3.7) by approximating the source term to the Taylor expansion of the center of $\left|\overline{BD}\right|$ and $\left|\overline{CD}\right|$. Here the index ℓ is the number of time that Eq. (3.9) has been iterated, and u_j^n solved by Eq. (3.8) can be denoted by $u_{j,0}^n$. Using the Cauchy criterion, we define the convergence as

$$\left|u_{j,\ell}^n - u_{j,\ell-1}^n\right| < \epsilon. \tag{3.10}$$

We stop the iterations if the convergence criterion is reached for a plausible small ϵ. The criterion is usually arrived within iterations less than ten times.

3.1.2 Convection-diffusion equation

In the momentum space, Eq. (2.13) can be transformed into

$$\frac{\partial \widetilde{u}}{\partial t} + (iap + \mu p^2)\widetilde{u} = 0, \tag{3.11}$$

by making the Fourier transformation. For simplicity, we just use the same symbol u instead of $\widetilde{u}$. The Eq. (3.11) becomes $\partial u/\partial t + (iap + \mu p^2)u = 0$. By using Gauss divergence theorem in E_2

$$\oint_{S(V)} \overrightarrow{h} \cdot d\overrightarrow{s} = -\int_V (iap + \mu p^2) u d\tau, \tag{3.12}$$

where $\overrightarrow{h}$ is defined by Eq. (3.5), too. Requirig that $u = u(p, t; j, n)$ defined by Eq. (3.4) satisfies Eq. (3.11) within $SE(j, n)$, one has

$$(u_t)_j^n = -(iap_j + \mu p_j^2) u_j^n. \tag{3.13}$$

The approximation of the total flux leaving the boundary of $CE_{\pm}(j, n)$ is

$$F_{\pm}(j, n) = \oint_{S(CE_{\pm}(j,n))} \overrightarrow{h} \cdot d\overrightarrow{s} = -i \int_{CE_{\pm}(j,n)} (iap + \mu p^2) u d\tau. \tag{3.14}$$

By Eqs. (3.4) and (3.14), the total flux leaving $CE_{\pm}(j, n)$ can be derived as

$$\begin{aligned} F_{\pm}(j, n) &= \frac{\triangle p}{2} \left\{ u_j^n \pm (u_{\overline{p}})_j^n - \left[(u)_{j\pm\frac{1}{2}}^{n-\frac{1}{2}} \mp (u_{\overline{p}})_{j\pm\frac{1}{2}}^{n-\frac{1}{2}} \right] \right\} \\ &= -(iap_{j\pm\frac{1}{4}} + \mu p_{j\pm\frac{1}{4}}^2) \left[(u)_{j\pm\frac{1}{2}}^{n-\frac{1}{2}} \mp (u_{\overline{p}})_{j\pm\frac{1}{2}}^{n-\frac{1}{2}} + \frac{\triangle t}{4} (u_t)_{j\pm\frac{1}{2}}^{n-\frac{1}{2}} \right] \frac{\triangle p}{2} \frac{\triangle t}{2}, \end{aligned} \tag{3.15}$$

where the conditions are similar to the previous simple wave problem. With the aid of Eqs. (3.15) and (3.13), u_j^n and $(u_{\overline{p}})_j^n$ can be solved iteratively in terms of $(u)_{j\pm\frac{1}{2}}^{n-\frac{1}{2}}$ and $(u_{\overline{p}})_{j\pm\frac{1}{2}}^{n-\frac{1}{2}}$. This explicit time-marching scheme is derived similar to the previous simple wave case. The iterating process can be added in the source term, too. But for the equation, it is not necessary to use the iterating process. So we do not go detail to describe it. For more details, we will show in the nonlinear chapter.

3.2 Boundary treatment

The boundary treatment in the momentum space CESE method is quite easy. Because the momentum is directly related to the kinetic energy, extremely large energy for a system is usually unphysical. So, only a moderate momentum region will be sufficient for numerical modeling. Also, the wave will simply vanish at the numerical boundary and cause no trouble like the methods in coordinate space. The non-reflecting boundary condition for momentum space CESE method is obtained in a simple way. That is when the numerical solution at the boundary, we add

the ghost cell. As depicted in Figure 2.5, we let

$$\begin{aligned} u^{n-\frac{1}{2}}_{j_{b+}+\frac{1}{2}} &= 0;\ u^{n-\frac{1}{2}}_{\overline{p}j_{b+}+\frac{1}{2}} = 0, \\ u^{n-\frac{1}{2}}_{j_{b-}-\frac{1}{2}} &= 0;\ u^{n-\frac{1}{2}}_{\overline{p}j_{b-}-\frac{1}{2}} = 0. \end{aligned} \tag{3.16}$$

, then there are CE_+ (with the ghost cell) and CE_- for $u^n_{j_{b+}}$ and $u^n_{\overline{p}j_{b+}}$ ($u^n_{j_{b-}}$ and $u^n_{\overline{p}j_{b-}}$).

Chapter 4 Nonlinear Problem

4.1 Korteweg-de Vries equation

The *Korteweg-de Vries* (KdV) equation is a classic example of the nonlinear system [16] The general form is

$$\frac{1}{\beta}\frac{\partial u}{\partial t} + \frac{\alpha}{\gamma}u\frac{\partial u}{\partial x} + \frac{1}{\gamma^3}\frac{\partial^3 u}{\partial x^3} = 0, \tag{4.1}$$

where α, β and γ are non-zero constants. The system contains both nonlinearity and dispersion. For convenience, we study in this section the scaled equation

$$\frac{\partial u}{\partial t} - 6u\frac{\partial u}{\partial x} + \frac{\partial^3 u}{\partial x^3} = 0. \tag{4.2}$$

By making the Fourier transformation and some manipulations, the momentum space equation is

$$\frac{\partial \widetilde{u}(p,t)}{\partial t} = 3ip\int_{-\infty}^{\infty}\widetilde{u}(q,t)\widetilde{u}(p-q,t)dq + ip^3\widetilde{u}(p,t). \tag{4.3}$$

For simplicity, we just use the same symbol u instead of $\widetilde{u}$. The Eq. (4.3) becomes $\partial u(p,t)/\partial t = 3ip\int_{-\infty}^{\infty}u(q,t)u(p-q,t)dq + ip^3u(p,t)$. Let $\overrightarrow{h} = (0,u)$ and apply the Gauss divergence theorem in E_2, Eq. (4.3) becomes

$$\oint_{S(V)}\overrightarrow{h}\cdot d\overrightarrow{s} = \int_V\left[3ip\int_{-\infty}^{\infty}u(q,t)u(p-q,t)dq + ip^3u(p,t)\right]d\tau, \tag{4.4}$$

where $d\tau = dpdt$. In the right-hand side of Eq. (4.4) is the source term. We can see that for a nonlinear system, the source term contains the convolution integral with unknown function. Hence the straightforward explicit iteration scheme described in previous section does not work. I implement two new ideas for the treatment of nonlinear problems in momentum space CESE method. First, at each time level, we calculate $u(p,t)$ and $\partial u(p,t)/\partial p$ at grids of half spacing, instead of spacing at $\triangle p$ in previous linear examples. Then the convolution integral can be calculated by the Simpson's rule [19]. Next, for every half-marching time step, say from $t^{n-\frac{1}{2}}$ to t^n, we begin by use u and u_p at $t^{n-\frac{1}{2}}$ for the source term to find the solution at t^n; then use the

obtained for source term calculation to generate new solution iteratively till the generated solution converged. Usually, the results converge within a few iterations.

To make it clear, from the conservation laws for $CE_{\pm}(j,n)$,

$$\oint_{S(CE_{\pm}(j,n))} \overrightarrow{h}(p,t;j,n)\cdot d\overrightarrow{s} = 3ip\int_{CE_{\pm}(j,n)}\left[\int_{-\infty}^{\infty} u(q,t)u(p-q,t)dq\right]d\tau + \int_{CE_{\pm}(j,n)} ip^3 u(p,t)d\tau, \tag{4.5}$$

where $\overrightarrow{h}(p,t;j,n) = (0, u(p,t;j,n))$. We can derive the following core scheme

$$\begin{aligned} u_j^n &= \frac{1}{2}\left\{[u-u_{\overline{p}}]_{j+\frac{1}{2}}^{n-\frac{1}{2}} + [u+u_{\overline{p}}]_{j-\frac{1}{2}}^{n-\frac{1}{2}}\right\} + \frac{F}{\triangle p} + \frac{G}{\triangle p}, \\ (u_{\overline{p}})_j^n &= \frac{1}{2}\left\{[u-u_{\overline{p}}]_{j+\frac{1}{2}}^{n-\frac{1}{2}} - [u+u_{\overline{p}}]_{j-\frac{1}{2}}^{n-\frac{1}{2}}\right\} + \frac{F}{\triangle p} - \frac{G}{\triangle p}, \end{aligned} \tag{4.6}$$

where we designated $u_j^n = u(p_j, t^n)$, $(u_{\overline{p}})_j^n \equiv \frac{\triangle p}{4}(u_p)_j^n$, and $\triangle\tau = \frac{\triangle t}{2}\frac{\triangle p}{2}$ for shorthand. And

$$\begin{cases} F = \left\{3ip_{i+\frac{1}{4}}\sum_j u(p_{i+\frac{1}{4}}-q, t^{n-\frac{1}{2}})u(q_j, t^{n-\frac{1}{2}})\frac{\triangle p}{2} + ip^3_{i+\frac{1}{4}}u(p_{i+\frac{1}{4}}, t^{n-\frac{1}{2}})\right\}\triangle\tau, \\ G = \left\{3ip_{i-\frac{1}{4}}\sum_j u(p_{i-\frac{1}{4}}-q, t^{n-\frac{1}{2}})u(q_j, t^{n-\frac{1}{2}})\frac{\triangle p}{2} + ip^3_{i-\frac{1}{4}}u(p_{i-\frac{1}{4}}, t^{n-\frac{1}{2}})\right\}\triangle\tau. \end{cases} \tag{4.7}$$

Here the value of $u(p_{i+\frac{1}{4}}, t^{n-\frac{1}{2}})$ is obtained by the Taylor expansion in the $SE(j, n-\frac{1}{2})$ or $SE(j\pm\frac{1}{2}, n-\frac{1}{2})$. It is obtained as

$$\begin{aligned} u(p_{i\pm\frac{1}{4}}, t^{n-\frac{1}{2}}) &= u(p_{i\pm\frac{1}{2}}, t^{n-\frac{1}{2}}) \mp u_{\overline{p}}(p_{i\pm\frac{1}{2}}, t^{n-\frac{1}{2}}) \\ \text{or } u(p_{i\pm\frac{1}{4}}, t^{n-\frac{1}{2}}) &= u(p_i, t^{n-\frac{1}{2}}) \pm u_{\overline{p}}(p_i, t^{n-\frac{1}{2}}). \end{aligned} \tag{4.8}$$

The value of $u(p_{i+\frac{1}{4}}-q, t^{n-\frac{1}{2}})$ may locate out of the computational domain in some specific value i and j. But there is no problem in the momentum space method. It is just to set zero when the node point is out of the domain. And all of the other values of $u(p_{i+\frac{1}{4}}-q, t^{n-\frac{1}{2}})$ are located at the numerical point for every i and j, when all of the half step grid is solved. The right-hand side of the Eq. (4.5) is called the source term, and for discrete form is defined as F and G for CE_+ and CE_-, respectively. But the value of u is centered in the space-time domain ($CE_{\pm}$). The former description is not correct. In the linear cases the centered value is just expanded as the Taylor expansion of space and time. But for this nonlinear case, the value of u_t is not trivial. So we must

impose the iterations to obtain the accurate solution. The iterating process is formed by renew the corresponding source term in the new value of u and $u_{\overline{p}}$. For more clear, we write down the iterating explicit scheme as

$$\begin{aligned} u^n_{j,\ell} &= \frac{1}{2}\left\{[u-u_{\overline{p}}]^{n-\frac{1}{2}}_{j+\frac{1}{2}} + [u+u_{\overline{p}}]^{n-\frac{1}{2}}_{j-\frac{1}{2}}\right\} + \frac{F_{\ell-1}}{\triangle p} + \frac{G_{\ell-1}}{\triangle p}, \\ (u_{\overline{p}})^n_{j,\ell} &= \frac{1}{2}\left\{[u-u_{\overline{p}}]^{n-\frac{1}{2}}_{j+\frac{1}{2}} - [u+u_{\overline{p}}]^{n-\frac{1}{2}}_{j-\frac{1}{2}}\right\} + \frac{F_{\ell-1}}{\triangle p} - \frac{G_{\ell-1}}{\triangle p}, \end{aligned} \tag{4.9}$$

where

$$\begin{aligned} F_{\ell-1} &= \\ &\left\{3ip_{i+\frac{1}{4}}\sum_j u_{\ell-1}(p_{i+\frac{1}{4}}-q,t^n)u_{\ell-1}(q_j,t^n)\frac{\triangle p}{2} + ip^3_{i+\frac{1}{4}}u_{\ell-1}(p_{i+\frac{1}{4}},t^n)\right\}\triangle\tau, \\ G_{\ell-1} &= \\ &\left\{3ip_{i-\frac{1}{4}}\sum_j u_{\ell-1}(p_{i-\frac{1}{4}}-q,t^n)u_{\ell-1}(q_j,t^n)\frac{\triangle p}{2} + ip^3_{i-\frac{1}{4}}u_{\ell-1}(p_{i-\frac{1}{4}},t^n)\right\}\triangle\tau, \end{aligned} \tag{4.10}$$

and $u_{\ell-1}(p_i,t^n) \equiv u^n_{j,\ell-1}$. The criterion of the above iterating process is defined as Eq. (3.10). The Eq. (4.9) is the final core-scheme for the KdV equation.

4.2 The Shock wave problem, Burgers's equation

In this section, we consider the Burgers's equation as an example of the nonlinear system and shock wave problem. The Burgers's equation is written as

$$\frac{\partial u}{\partial t} + u\frac{\partial u}{\partial x} = \upsilon\frac{\partial^2 u}{\partial x^2}\ (\upsilon > 0). \tag{4.11}$$

In Burgers's equation the term on the right may be interpreted as a dissipative effect; namely as the removal of energy from the system desribed by the equation. Burgers's equation serves to model a gas shock wave in which energy dissipation is present ($\upsilon > 0$). The steepening effect of nonlinearity in the second term on the left can be balanced by the dissipative effect, leading to a traveling wave of constant form, unlike the case corresponding to $\upsilon = 0$ in which a smooth initial condition evolved into a discontinuous solution (shock). The steady traveling wave solution for Burgers's equation is the so-called Burgers's shock wave.

By making the Fourier transformation and some manipulations, the momentum space equation

is

$$\frac{\partial \widetilde{u}(p,t)}{\partial t} = -\frac{1}{2} ip \int_{-\infty}^{\infty} \widetilde{u}(q,t)\widetilde{u}(p-q,t)dq - \upsilon p^2 \widetilde{u}(p,t). \tag{4.12}$$

For simplicity, we just use the same symbol u instead of $\widetilde{u}$. The Eq. (4.12) becomes $\partial u(p,t)/\partial t = -\frac{1}{2} ip \int_{-\infty}^{\infty} u(q,t)u(p-q,t)dq - \upsilon p^2 u(p,t)$. Let $\overrightarrow{h} = (0,u)$ and apply the Gauss divergence theorem in E_2, Eq. (4.12) becomes

$$\oint_{S(V)} \overrightarrow{h} \cdot d\overrightarrow{s} = \int_V \left[-\frac{1}{2} ip \int_{-\infty}^{\infty} u(q,t)u(p-q,t)dq - \upsilon p^2 u(p,t) \right] d\tau, \tag{4.13}$$

where $d\tau = dpdt$. From the conservation laws for $CE_{\pm}(j,n)$,

$$\oint_{S(CE_{\pm}(j,n))} \overrightarrow{h}(p,t;j,n) \cdot d\overrightarrow{s} = -\frac{1}{2} ip \int_{CE_{\pm}(j,n)} \left[\int_{-\infty}^{\infty} u(q,t)u(p-q,t)dq \right] d\tau - \int_{CE_{\pm}(j,n)} \upsilon p^2 u(p,t) d\tau, \tag{4.14}$$

where $\overrightarrow{h}(p,t;j,n) = (0, u(p,t;j,n))$. We can derive the following core scheme same as Eq. (4.6), where we also designated $u_j^n = u(p_j, t^n)$, $(u_{\overline{p}})_j^n \equiv \frac{\triangle p}{4}(u_p)_j^n$, and $\triangle\tau = \frac{\triangle t}{2}\frac{\triangle p}{2}$ for shorthand. And

$$\begin{aligned} F &= \left\{ -\frac{1}{2} ip_{i+\frac{1}{4}} \sum_j u(p_{i+\frac{1}{4}} - q_j, t^{n-\frac{1}{2}}) u(q_j, t^{n-\frac{1}{2}}) \frac{\triangle p}{2} - \upsilon p_{i+\frac{1}{4}}^2 u(p_{i+\frac{1}{4}}, t^{n-\frac{1}{2}}) \right\} \triangle\tau, \\ G &= \left\{ -\frac{1}{2} ip_{i-\frac{1}{4}} \sum_j u(p_{i-\frac{1}{4}} - q_j, t^{n-\frac{1}{2}}) u(q_j, t^{n-\frac{1}{2}}) \frac{\triangle p}{2} - \upsilon p_{i-\frac{1}{4}}^2 u(p_{i-\frac{1}{4}}, t^{n-\frac{1}{2}}) \right\} \triangle\tau. \end{aligned} \tag{4.15}$$

Here the value of $u(p_{i+\frac{1}{4}}, t^{n-\frac{1}{2}})$ is obtained by the Taylor expansion in the $SE(j, n-\frac{1}{2})$ or $SE(j \pm \frac{1}{2}, n-\frac{1}{2})$, too. The value of $u(p_{i+\frac{1}{4}} - q, t^{n-\frac{1}{2}})$ may locate out of the computational domain in some specific value i and j. It is just to set zero as before. And all of the other values of $u(p_{i+\frac{1}{4}} - q, t^{n-\frac{1}{2}})$ are treated in the same way. The right-hand side of the Eq. (4.14) is called the source term, and for discrete form is defined as F and G for CE_+ and CE_-, respectively. But the value of u is centered in the space-time domain ($CE_{\pm}$). The iterative process is used for this problem, too. The iterating process is formed by updating the corresponding source term in the

new value of u and $u_{\overline{p}}$. For more clear, we write down the iterating explicit scheme as Eq. (4.9), where

$$F_{\ell-1} = \left\{ -\frac{1}{2} i p_{i+\frac{1}{4}} \sum_j u_{\ell-1}(p_{i+\frac{1}{4}} - q_j, t^n) u_{\ell-1}(q_j, t^n) \frac{\triangle p}{2} - \upsilon p^2_{i+\frac{1}{4}} u_{\ell-1}(p_{i+\frac{1}{4}}, t^n) \right\} \triangle \tau, \tag{4.16}$$

$$G_{\ell-1} = \left\{ -\frac{1}{2} i p_{i-\frac{1}{4}} \sum_j u_{\ell-1}(p_{i-\frac{1}{4}} - q_j, t^n) u_{\ell-1}(q_j, t^n) \frac{\triangle p}{2} - \upsilon p^2_{i-\frac{1}{4}} u_{\ell-1}(p_{i-\frac{1}{4}}, t^n) \right\} \triangle \tau,$$

and $u_{\ell-1}(p_i, t^n) \equiv u^n_{j,\ell-1}$. The criterion of the above iterative process is defined as Eq. (3.10). The Eq. (4.9) is the final core-scheme for the Burgers's equation, too.

Chapter 5 Non-uniform grid Momentum Space CESE Method

The non-uniform grid momentum space CESE method is developed in this chapter. The main goal is to treat Burgers's equation for less grid points. The solution of Burgers's equation has a shock in center of domain. Dense grid near the shock region is necessary to capture the shock.

5.1 Basic derivation

Consider the space-time mesh ($-L \le x \le L$ and $t \ge 0$) depicted in Figure 5.1. Here (i) $L > 0$ is a given length, and (ii) the mesh structure in the region $-L \le x \le 0$ is the mirror image of that in the region $0 \le x \le L$. Let the domain $0 \le x \le L$ on the x-coordinate line be divided into K intervals using the dividing coordinate points $\widehat{x}_1, \widehat{x}_2, ..., \widehat{x}_{K-1}$ where

$$0 < \widehat{x}_1 < \widehat{x}_2 < ... < \widehat{x}_{K-1} < L. \tag{5.1}$$

Let

$$L_k \equiv \widehat{x}_k - \widehat{x}_{k-1},\ k = 1, 2, ..., K \tag{5.2}$$

with

$$\widehat{x}_0 \equiv 0 \text{ and } \widehat{x}_K \equiv L. \tag{5.3}$$

Then

$$\sum_{k=1}^{K} L_k = L, \text{ and } L_k > 0,\ k = 1, 2, ..., K. \tag{5.4}$$

Moreover, for any k, let the interval $(\widehat{x}_{k-1}, \widehat{x}_k)$ be divided into M uniform sub-intervals with the dividing points $\widehat{x}_{k-1}^{(1)}, \widehat{x}_{k-1}^{(2)}, ..., \widehat{x}_{k-1}^{(M-1)}$ where $M > 0$ is a given integer and

$$\widehat{x}_{k-1} < \widehat{x}_{k-1}^{(1)} < \widehat{x}_{k-1}^{(2)} < ... < \widehat{x}_{k-1}^{(M-1)} < \widehat{x}_k. \tag{5.5}$$

Thus

$$\widehat{x}_{k-1}^{(m)} - \widehat{x}_{k-1}^{(m-1)} = \ell_k,\ m = 1, 2, ..., M \tag{5.6}$$

where

$$\widehat{x}_{k-1}^{(0)} \equiv \widehat{x}_{k-1} \text{ and } \widehat{x}_{k-1}^{(M)} \equiv \widehat{x}_k. \tag{5.7}$$

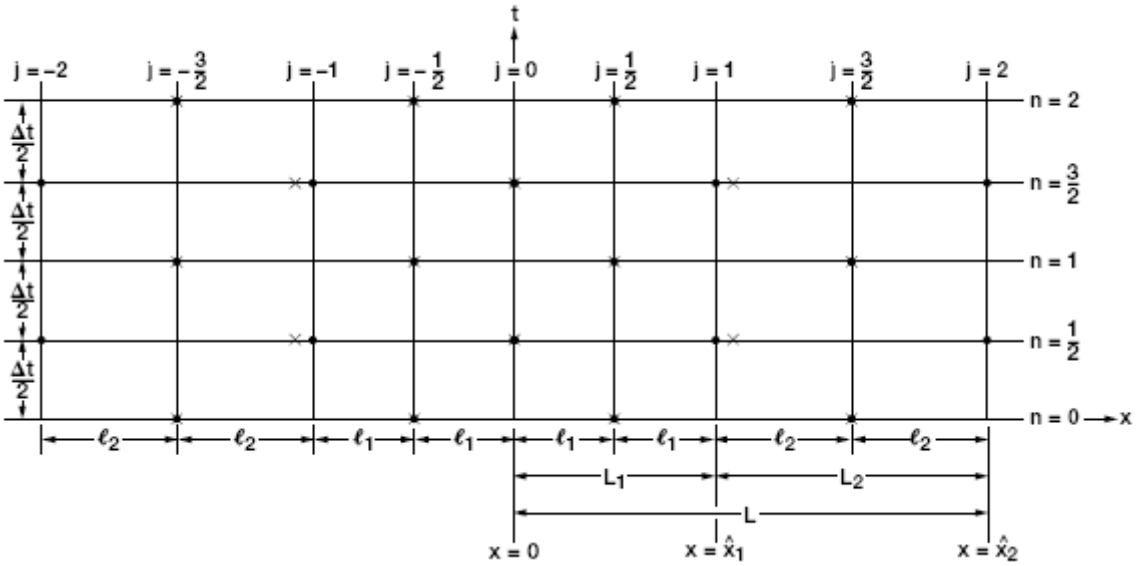

Figure 5.1: A space-time mesh with nonuniform spatial intervals ($K = M = 2$).

For our discussion, M is usually 2.

Consider the PDE given in Eq. (4.12), and apply the conservation laws in the unity space-time domain. The similar equation Eq. (4.13) is followed. The $CE_+(j,n)$ and $CE_-(j,n)$ with the different size of the spatial domain, but the conservation laws are never changed. From the conservation laws for $CE_\pm(j,n)$,

$$\oint_{S(CE_\pm(j,n))} \overrightarrow{h}(p,t;j,n)\cdot d\overrightarrow{s} = -\frac{1}{2}ip\int_{CE_\pm(j,n)}\left[\int_{-\infty}^{\infty} u(q,t)u(p-q,t)dq\right]d\tau - \int_{CE_\pm(j,n)} \upsilon p^2 u(p,t)d\tau, \tag{5.8}$$

where $\overrightarrow{h}(p,t;j,n) = (0, u(p,t;j,n))$. The CE and SE is depicted in Figure 5.2. For any $(x,t) \in SE(j,n)$, $u(x,t)$, and $\overrightarrow{h}(x,t)$ are approximated by $u(x,t;j,n)$ and $\overrightarrow{h}(x,t;j,n)$, respectively. Using the first order Taylor's expansion of $u(x,t)$ at (x_j, t^n), we define

$$u(x,t;j,n) = u_j^n + (u_x)_j^n(x - x_j) + (u_t)_j^n(t - t^n). \tag{5.9}$$

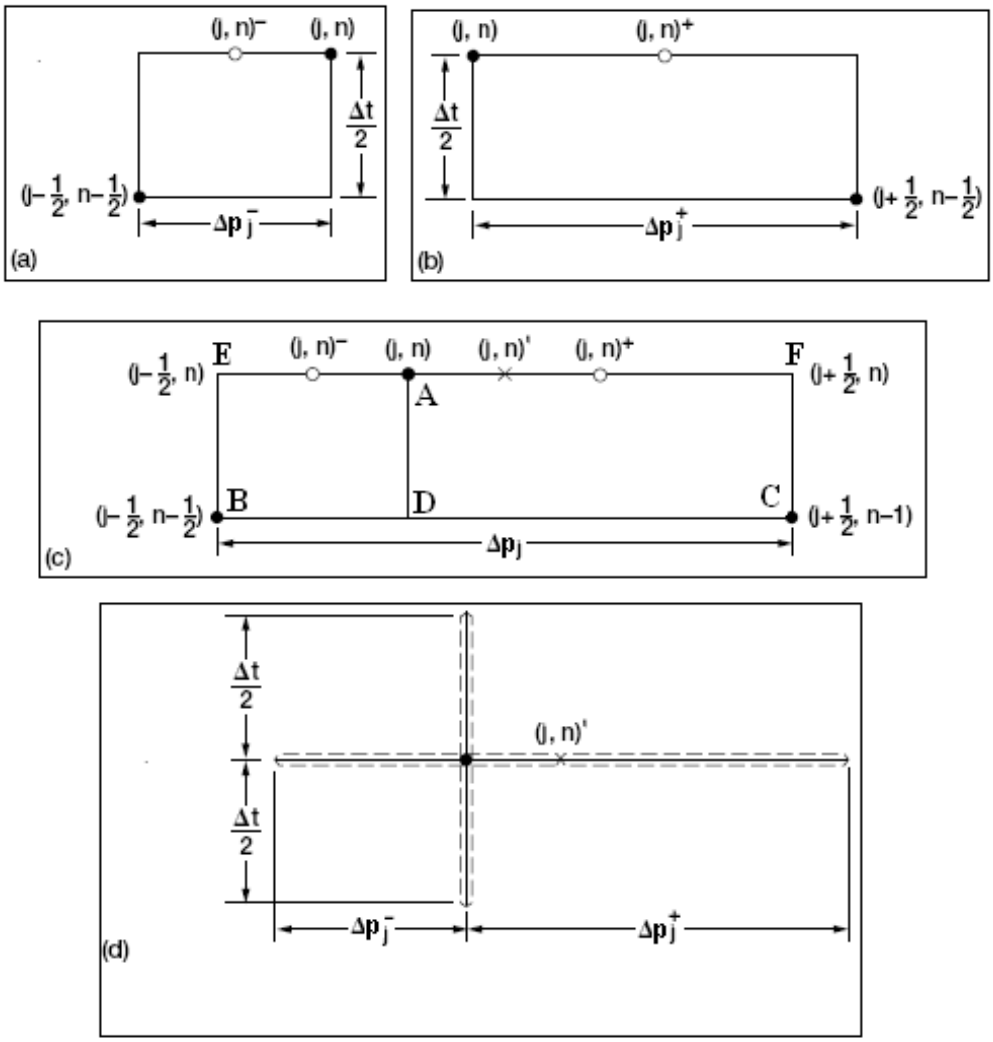

Figure 5.2: The SE and CE for a non-uniform mesh. (a) $CE_{-}(j,n)$. (b) $CE_{+}(j,n)$. (c) $CE(j,n)$. (d)$SE(j,n)$.

Let $\left|\overline{CD}\right| = \frac{\triangle p_j^+}{2}$ and $\left|\overline{BD}\right| = \frac{\triangle p_j^-}{2}$ We can derive the following conservation laws: $CE_+ \Rightarrow$

$$\left[u_j^n + \frac{\triangle p_j^+}{4}(u_p)_j^n - u_{j+\frac{1}{2}}^{n-\frac{1}{2}} + \frac{\triangle p_j^+}{4}(u_p)_{j+\frac{1}{2}}^{n-\frac{1}{2}}\right]\frac{\triangle p_j^+}{2} \tag{5.10}$$

$$= \left[-\frac{1}{2}ip_{i+\frac{1}{4}}\sum_j u(p_{i+\frac{1}{4}} - q_j, t^{n-\frac{1}{2}})u(q_j, t^{n-\frac{1}{2}})\frac{\triangle p_j}{2} - \upsilon p_{i+\frac{1}{4}}^2 u(p_{i+\frac{1}{4}}, t^{n-\frac{1}{2}})\right]\frac{\triangle p_j^+}{2}\frac{\triangle t}{2}.$$

$CE_- \Rightarrow$

$$\left[u_j^n - \frac{\triangle p_j^-}{4}(u_p)_j^n - u_{j-\frac{1}{2}}^{n-\frac{1}{2}} - \frac{\triangle p_j^+}{4}(u_p)_{j-\frac{1}{2}}^{n-\frac{1}{2}}\right]\frac{\triangle p_j^-}{2} \tag{5.11}$$

$$= \left[-\frac{1}{2}ip_{i-\frac{1}{4}}\sum_j u(p_{i-\frac{1}{4}} - q_j, t^{n-\frac{1}{2}})u(q_j, t^{n-\frac{1}{2}})\frac{\triangle p_j}{2} - \upsilon p_{i-\frac{1}{4}}^2 u(p_{i-\frac{1}{4}}, t^{n-\frac{1}{2}})\right]\frac{\triangle p_j^-}{2}\frac{\triangle t}{2}.$$

Let

$$F \equiv \tag{5.12}$$

$$\left[-\frac{1}{2}ip_{i+\frac{1}{4}}\sum_j u(p_{i+\frac{1}{4}} - q_j, t^{n-\frac{1}{2}})u(q_j, t^{n-\frac{1}{2}})\frac{\triangle p_j}{2} - \upsilon p_{i+\frac{1}{4}}^2 u(p_{i+\frac{1}{4}}, t^{n-\frac{1}{2}})\right]\frac{\triangle p_j^+}{2}\frac{\triangle t}{2},$$

$$G \equiv$$

$$\left[-\frac{1}{2}ip_{i-\frac{1}{4}}\sum_j u(p_{i-\frac{1}{4}} - q_j, t^{n-\frac{1}{2}})u(q_j, t^{n-\frac{1}{2}})\frac{\triangle p_j}{2} - \upsilon p_{i-\frac{1}{4}}^2 u(p_{i-\frac{1}{4}}, t^{n-\frac{1}{2}})\right]\frac{\triangle p_j^-}{2}\frac{\triangle t}{2},$$

and

$$F' \equiv \frac{2}{\triangle p_j^+}F; G' \equiv \frac{2}{\triangle p_j^-}G. \tag{5.13}$$

We define

$$\nu_- \equiv \frac{1}{4}\triangle p_j^- \text{ and } \nu_+ = \frac{1}{4}\triangle p_j^+ \tag{5.14}$$

for simplify our description. The Eq. (5.13) becomes $F' \equiv \frac{1}{2\nu_+}F; G' \equiv \frac{1}{2\nu_-}G$. The core scheme is formed by an explicit way as

$$\begin{aligned} u_j^n &= \frac{1}{\nu_- + \nu_+}\left\{\nu_- u_{j+\frac{1}{2}}^{n-\frac{1}{2}} - \nu_-\nu_+(u_p)_{j+\frac{1}{2}}^{n-\frac{1}{2}} + \nu_+ u_{j-\frac{1}{2}}^{n-\frac{1}{2}} + \nu_-\nu_+(u_p)_{j-\frac{1}{2}}^{n-\frac{1}{2}}\right\} \\ &\quad + \frac{\nu_- F'}{\nu_- + \nu_+} + \frac{\nu_+ G'}{\nu_- + \nu_+} \\ (u_p)_j^n &= \frac{1}{\nu_- + \nu_+}\left\{u_{j+\frac{1}{2}}^{n-\frac{1}{2}} - \nu_+(u_p)_{j+\frac{1}{2}}^{n-\frac{1}{2}} - u_{j-\frac{1}{2}}^{n-\frac{1}{2}} - \nu_-(u_p)_{j-\frac{1}{2}}^{n-\frac{1}{2}}\right\} \\ &\quad + \frac{F'}{\nu_- + \nu_+} - \frac{G'}{\nu_- + \nu_+} \end{aligned} \tag{5.15}$$

The value of $u(p_{i+\frac{1}{4}}, t^{n-\frac{1}{2}})$ is used in the similar way as before, and the convolution treatment is

similar,too. But a trouble occurs in computing the value of $u(p_{i+\frac{1}{4}} - q_j, t^{n-\frac{1}{2}})$. The values for most i and j are not in the numerical nodes. In orther word, we do not have these numerical data. It is much difficult and complicated than uniform grid problem. Some people will say it can be interpolated by the known data. This is not I want to do. The CESE method compute flux in a simple way. If I use interpolation to solve these values, I will violate the main idea of CESE method. So I uses the nearest node to expand these points in SE. It is obtained in the similar way about the flux computation, i.e. use the Taylor expansion from the solution element. The non-uniform grid momentum space CESE method is consistent for previous CESE method. The right-hand side of the Eq. (5.10) and Eq. (5.11) is called the source term, and for discrete form is defined as F and G for CE_+ and CE_-, respectively. But the above interpretation is not correct for the source term calculation. The value of u is centered in the space-time domain ($CE_\pm$). So the Eq. (5.15) is modified by an iterating processing as

$$\begin{aligned} u^n_{j,\ell} &= \frac{1}{\nu_- + \nu_+}\left\{\nu_- u^{n-\frac{1}{2}}_{j+\frac{1}{2}} - \nu_-\nu_+ (u_p)^{n-\frac{1}{2}}_{j+\frac{1}{2}} + \nu_+ u^{n-\frac{1}{2}}_{j-\frac{1}{2}} + \nu_-\nu_+ (u_p)^{n-\frac{1}{2}}_{j-\frac{1}{2}}\right\} \\ &+ \frac{\nu_- F'_{\ell-1}}{\nu_- + \nu_+} + \frac{\nu_+ G'_{\ell-1}}{\nu_- + \nu_+}, \\ (u_{\overline{p}})^n_{j,\ell} &= \frac{1}{\nu_- + \nu_+}\left\{u^{n-\frac{1}{2}}_{j+\frac{1}{2}} - \nu_+ (u_p)^{n-\frac{1}{2}}_{j+\frac{1}{2}} - u^{n-\frac{1}{2}}_{j-\frac{1}{2}} - \nu_- (u_p)^{n-\frac{1}{2}}_{j-\frac{1}{2}}\right\} \\ &+ \frac{F'_{\ell-1}}{\nu_- + \nu_+} - \frac{G'_{\ell-1}}{\nu_- + \nu_+}, \end{aligned} \tag{5.16}$$

where

$$\begin{aligned} F_{\ell-1} &= \\ &\left\{-\frac{1}{2} i p_{i+\frac{1}{4}} \sum_j u_{\ell-1}(p_{i+\frac{1}{4}} - q_j, t^n) u_{\ell-1}(q_j, t^n) \frac{\triangle p_j}{2} - \upsilon p^2_{i+\frac{1}{4}} u_{\ell-1}(p_{i+\frac{1}{4}}, t^n)\right\} \frac{\triangle p^+_j}{2} \frac{\triangle t}{2}, \end{aligned} \tag{5.17}$$

$$\begin{aligned} G_{\ell-1} &= \\ &\left\{-\frac{1}{2} i p_{i-\frac{1}{4}} \sum_j u_{\ell-1}(p_{i-\frac{1}{4}} - q_j, t^n) u_{\ell-1}(q_j, t^n) \frac{\triangle p_j}{2} - \upsilon p^2_{i-\frac{1}{4}} u_{\ell-1}(p_{i-\frac{1}{4}}, t^n)\right\} \frac{\triangle p^-_j}{2} \frac{\triangle t}{2}. \end{aligned}$$

and $u_{\ell-1}(p_i, t^n) \equiv u^n_{j,\ell-1}$. The criterion of the above iterating process is defined as Eq. (3.10). The Eq. (5.16) is the core-scheme for the non-uniform grid momentum space CESE method.

5.2 A special technique to approve the accuracy

The non-uniform grid momentum space CESE method is described in the before section. The convolution integral is computed by the simple Riemann integral. If we want more accurate of the convolution integral, the Gauss-Chebyshev-Lobatto quadrature is required. The motivation of this section is to decreasing the iterating steps. The more accurate convolution integral will decreasing the iterating steps, and makes this non-uniform grid method more effectively.

The Gauss-Chebyshev-Lobatto grid is described as

$$\begin{aligned} \theta_j &= \frac{N-j}{N}\pi, \quad j = 0, 1, 2, ..., N,\ \theta_j \in [\pi, 0] \\ y_j &= \cos(\theta_j) \ \in [-1, 1] \\ q_j &= R \cdot y_j \ \in [-R, R] \end{aligned} \tag{5.18}$$

The quadrature formula is

$$\int_{-R}^{R} F(q)dq = R\int_{-1}^{1} F(Ry)dy = R\sum_{j=0}^{N} w_j F(Ry_j)\sqrt{1-y_j^2} \tag{5.19}$$

where

$$w_j = \begin{cases} \frac{\pi}{2N}, & j = 0, N \\ \frac{\pi}{N}, & j = 1, 2, ..., N-1 \end{cases} \tag{5.20}$$

The convolution integral in Eq. (5.8) is

$$\int_{-\infty}^{\infty} u(q,t)u(p-q,t)dq. \tag{5.21}$$

Without loss of generality, we let the computation domain to be $[-R, R]$ Eq. (5.21) becomes

$$\int_{-R}^{R} u(q,t)u(p-q,t)dq. \tag{5.22}$$

We use the basic idea of the calculas "change of variable". The Eq. (5.22) becomes

$$\begin{aligned} \int_{-R}^{R} u(q,t)u(p-q,t)dq &= R\int_{-1}^{1} u(Ry,t)u(p-Ry,t)dy. \\ &= R\sum_{j=0}^{N} w_j u(Ry_j,t)u(p-Ry_j,t)\sqrt{1-y_j^2} \end{aligned} \tag{5.23}$$

where θ_j, r_j, w_j are defined in Eq. (5.18). This convolution integral is computed in the Gauss-Chebyshev-Lobatto quadrature. But it is not I want, the grids is not dense in center but

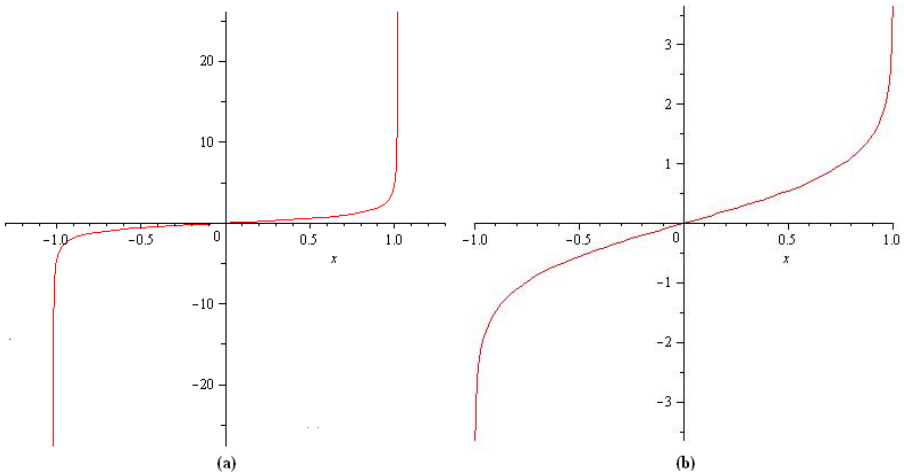

Figure 5.3: The transformation function for non-uniform grid momentum space CESE method. (a).The Eq. (5.21) (b).The Eq. (5.22).

dense in boundary. We introduce a new way of change of variabe to obtain the dense grids in center. And it is transformed to Gauss-Chebyshev-Lobatto grids, too. Let

$$q = \frac{y}{\sqrt{\frac{(1+R^2)}{R^2} - y^2}},\ y \in [-1, 1]\,;\ x \in [-R, R]\,. \tag{5.24}$$

We use the Gauss-Chebyshev-Lobatto grids to generate y_j, $j = 1, 2, ..., N$. The transformation defined in Eq. (5.24) transform the Gauss-Chebyshev-Lobatto grids to the dense grids in center. Then Eq. (5.22) can be solved in

$$\int_{-R}^{R} u(q,t)u(p-q,t)dq = R\int_{-1}^{1} u(\frac{y}{\sqrt{\frac{(1+R^2)}{R^2} - y^2}}, t)u(p - \frac{y}{\sqrt{\frac{(1+R^2)}{R^2} - y^2}}, t)\frac{dq}{dy}dy.$$

where $\frac{dq}{dy} = \frac{d}{dy}\left(\frac{y}{\sqrt{\frac{(1+R^2)}{R^2} - y^2}}\right)$. The Gauss-Chebyshev-Lobatto quadrature is solved in a similar way. We introduce the another transformation as

$$x = \tanh^{-1}(\tanh(R)y),\ y \in [-1, 1]\,;\ x \in [-R, R]\,. \tag{5.25}$$

These two transformation function are depicted in Figure 5.3.

Chapter 6 A Quantum Mechanical Problem

The momentum space time dependent Schrödinger equation (TDSE) with intense laser pulse is described as

$$i\frac{\partial}{\partial t}|\psi\rangle = \frac{p^2}{2}|\psi\rangle + V(p)|\psi\rangle - qA(t)p|\psi\rangle \tag{6.1}$$

where V : potential, A : vector potential and q : electric charge. This is the dimensionless form, and the electric charge $q = -1$ for electron. The TDSE we considered here is the single atom, single-active electron system.

We use the so-called "soft-Coulomb" potential (Figure 6.1) which behaves asympotically as a one-dimensional Coulomb potential and supports an infinite number of bound states. The "soft-Coulomb" potential is defined as

$$V(x) = -\frac{1}{\sqrt{c - x^2}}. \tag{6.2}$$

With $c = 1.41$, the ground-state energy is the same as for Ar atoms: $\epsilon_0 = -0.58$ a.u. This class of potentials has been shown to be useful to reproduce the main features of laser-atom interactions in the strong-field regime, for a linearly polarized laser. The corresponding momentum space potential is defined as

$$V(p) = \begin{cases} -\frac{1}{\pi}K_0(\sqrt{c}\,|p|), & p \neq 0 \\ -\frac{1}{\pi}\ln(R + \sqrt{R^2 + c}) + \frac{1}{2\pi}\ln(c), & p = 0 \end{cases} \tag{6.3}$$

where K_0 is the modified Bessel function of the 2[nd] kind.

The electric field is choosed by a practical $\sin^2$ pluse ,

$$E(t) = E_0 \sin(\omega t)\sin^2(\frac{\pi t}{T}),\ t \in [0, T]\,. \tag{6.4}$$

The vector potential is defined by $E(t) = -\frac{\partial}{\partial t}A(t)$ (see Figure 6.2),

$$A(t) = \frac{E_0}{2\omega}\cos(\omega t) - \frac{E_0}{4}\left[\frac{\cos(\omega + \Omega)t}{\omega + \Omega} + \frac{\cos(\omega - \Omega)t}{\omega - \Omega}\right] + \frac{E_0}{2}\frac{\Omega^2}{\omega(\omega^2 - \Omega^2)} \tag{6.5}$$

where $\Omega = \frac{2\pi}{T}$.

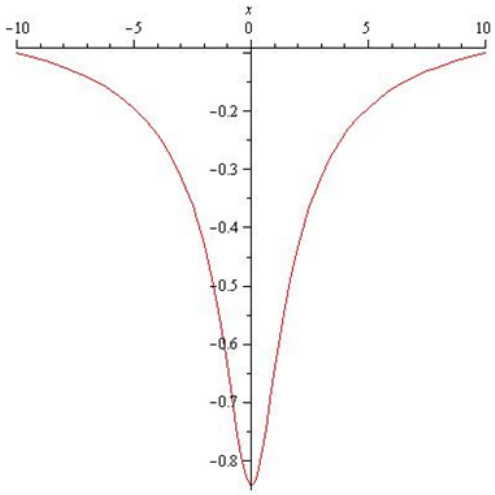

Figure 6.1: The soft-Coulomb potential.

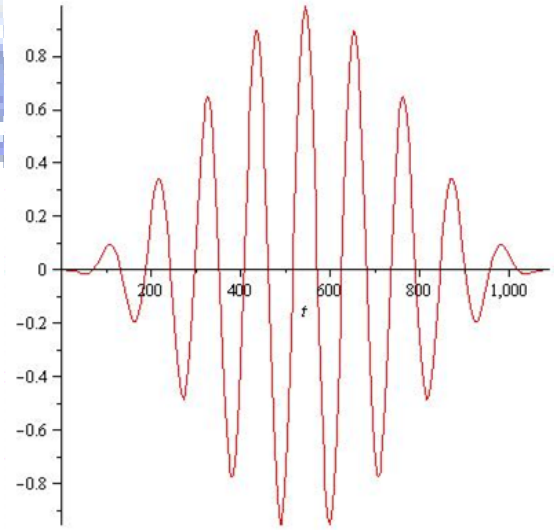

Figure 6.2: The vector potential.

When atoms are submitted to intense infrared laser pulses with peak intensities around $I \approx 10^{14} W cm^{-2}$, the energy distributions of the fast photoelectrons can exhibit strong variations, up to one-(or even two-) order(s) of magnitude, when the peak intensity changes by only a few percents. Soon, it was realized that these effects could be related to the structure of the atomic system considered. This was clearly evidenced in a series of papers devoted to the interpretation of experiments conducted on Ar atoms submitted to Ti: sapphire laser pulses ($\omega = 0.0577$ a.u. and time durations $T \approx 120$ f.s.) Indeed, by solving the time-dependent Schrödinger equation (TDSE) for a model argon atom, it has been possible to reproduce the high-energy structures in the photoelectron spectra with remarkable agreement.

6.1 Steady state problem

At the beginning of simulation, we must have the ground state wave function. The static state Schrödinger equation must be solved.

$$\left(\frac{p^2}{2} + V(x)\right)|\psi\rangle = E\,|\psi\rangle \tag{6.6}$$

We introduced a simple man method to let problem into the eigenvalue problem.

$$\frac{p_i^2}{2}\psi(p_i) + \triangle p \sum_j V(p_i - p_j)\psi(p_j) = E\psi(p_i) \tag{6.7}$$

This becomes an eigenvalue problem ($AX = \lambda X$). In this article, we use the QZ algorithm or JD solver to solve this problem. For large scale problem, the JD solver has been shows it excellent talent.

6.2 Time evolution, using momentum space CESE method

The discrete form of Eq. (6.1) is

$$i\frac{\partial}{\partial t}\psi(p_j, t) = \left(\frac{p_j^2}{2} - qA(t)p_j\right)\psi(p_j, t) + \sum_k V(p_j - p_k)\triangle p\psi(p_k, t) \tag{6.8}$$

It can be transform to

$$\frac{\partial}{\partial t}\psi(p_j, t) = -i\left(\frac{p_j^2}{2} - qA(t)p_j\right)\psi(p_j, t) - i\sum_k V(p_j - p_k)\triangle p\psi(p_k, t) \tag{6.9}$$

The momentum space CESE method for this case can also be derived. And the explicit scheme is

derived in the similar way. The iterating explicit scheme is same as Eq. (4.9). But the source term must be changed to the right-hand side of Eq. (6.9). The derivation is completely similar, so we do not derive it again.

6.3 Renormalization

At the end of the simulation we obtain the final state wave function $\psi(p_i) = \langle p_i|\psi\rangle$ which we map onto the energy eigenstates: $\psi(E_i) = \langle E_i|p_i\rangle \langle p_i|\psi\rangle$ where the matrix $\langle E_i|p_i\rangle$ are the eigenvectors of the Hamiltonian $\left\langle p_i'|H|p_i\right\rangle = \left\langle p_i'|E_i'\right\rangle \left\langle E_i'|H|E_i\right\rangle \langle E_i|p_i\rangle$. (Note that for continuous states, $\pm p_i$ correspond to the same $E_i \sim \frac{p_i^2}{2}$.) The middle matrix is the diagonalized Hamiltonian. At this point, the state vector has the normalization

$$\sum\nolimits_i |\langle E_i|\psi\rangle|^2 = 1.$$

For positive energies, we interpolate this discrete state $\psi\left(E_i\right)$ onto a continuous probability function $\mathrm{Prob}(E)$ using a step function mapping:

$$\mathrm{Pr\,ob}(E) = \sum\nolimits_i |\langle E_i|\psi\rangle|^2 \times h\left(E_{i+\frac{1}{2}} - E\right) \times h\left(E - E_{i-\frac{1}{2}}\right) / \left(E_{i+\frac{1}{2}} - E_{i-\frac{1}{2}}\right).$$

Here $h\left(x\right)$ is the Heaviside function $h(x > 0) = 1$ and $h(x < 0) = 0$. The half interval energy $E_{i+\frac{1}{2}} \equiv \frac{E_{i+\frac{1}{2}} - E_{i-\frac{1}{2}}}{2}$. This continuous function $\mathrm{Prob}(E)$ now has the correct probability normalization. And $\int_0^\infty \mathrm{Prob}(E)dE$, can be interpreted as the probability per unit energy (in atomic units) of finding an ionized electron.

Chapter 7 Numerical Results for basic problems

All of the one-dimensional PDEs described in the previous section are tested using appropriate model problems. The coordinate space and momentum space CESE method are tested with respect to different kind of PDE. The numerical results are compared with the analytic solution to examine their accuracy. Here we present the error analysis for this method. We define the root-mean-square error at final moment as follow:

$$E(\triangle x) = \sqrt{\frac{1}{N}\sum_{j=0}^{N}(u(x_j, t^{final}) - u_{exact})^2}, \tag{7.1}$$

$$E(\triangle p) = \sqrt{\frac{1}{N}\sum_{j=0}^{N}(u(p_j, t^{final}) - u_{exact})^2}.$$

For the quantum mechanical problem described in previous section, it has no analytic solution about it. The numerical result of the stationary state energy is showed to examine their accuracy. Here we can compare the results about our simulation with several results proposed at other papers [13][14].

7.1 Coordinate space CESE Method

7.1.1 The a-scheme and the c-scheme

Consider the first-order wave equation Eq. (2.1) where $a = 5$ in the domain $-5 \leq x \leq 5$. The initial condition is described as

$$u(x,0) = \begin{cases} \sin(\omega x), & x \in [-1,1] \\ 0 \ , \text{ others} \end{cases} \tag{7.2}$$

or

$$u(x,0) = c_1 \exp(\frac{-(x-c_2)^2}{2c_3^2}) \tag{7.3}$$

where $\omega = 2\pi$, $c_1 = 0$, $c_2 = 0$, $c_3 = 1$ (c_1: height of the Gaussian peak, c_2: position of the center of the peak, c_3: width of the bump). With non-reflecting boundary condition imposed at $x = -5$

and $x = 5$, the exact solution is

$$u_e(x,t) = \begin{cases} \sin(\omega(x-at)), & x-at \in [-1,1] \\ 0 \quad , \text{ others} \end{cases} \tag{7.4}$$

or

$$u(x,t) = c_1 \exp(\frac{-((x-at)-c_2)^2}{2c_3^2}) \tag{7.5}$$

This problem is solved by using the CESE a-scheme and c-scheme, respectively. The problem here we considered with the Courant number (CFL) is 0.25, $\triangle x = 0.01$, $\triangle t = 0.0005$ and time duration $T = 1$. The numerical results for the a-scheme are depicted in Figure 7.1 and Figure 7.2. And the numerical results for the c-scheme are depicted in Figure 7.3 and Figure 7.4.

7.1.2 The a-μ scheme

The a-μ scheme is used to solve the convection-diffusion equation Eq. (2.13) where $a = 5$ and $\mu = 0.1$ in the domain $-5 \leq x \leq 5$. The initial condition is described as Eq. 7.3 with the coefficient $c_1 = \frac{1}{\sqrt{2}}$, $c_2 = 0$, $c_3 = \sqrt{2}$. With non-reflecting boundary condition imposed at $x = -5$ and $x = 5$, the exact solution is

$$u(x,t) = \frac{c_1}{\sqrt{1+\mu t}} \exp(\frac{-((x-at)-c_2)^2}{2c_3^2(1+\mu t)}) \tag{7.6}$$

The problem here we considered with the Courant number (CFL) is 0.25, $\triangle x = 0.01$, $\triangle t = 0.0005$ and time duration $T = 2$. The numerical results for the a-μ scheme are depicted in Figure 7.5. It shows the second-order scheme is not works well. So, the higher-order scheme is necessary.

7.1.3 The wiggle-suppressing scheme

If discontinuities, non-differentiable, or shocks are presented in a numerical solution, any scheme introduced in above section is not equipped to suppress numerical wiggles that generally appear near these points. This extension scheme is called $w-\alpha$ scheme which is introduced as a remedy for this deficiency. We use the extension of the c-τ^* scheme introduced in above section. The simplest function of the c-τ^* scheme results from the choice $f(s) = \sqrt{s}$, i.e.,

$\tau = f(\nu^2) = |\nu|$, where $|\nu| < 1$. We use the condition as Sec. 7.1.1. In Figure 7.6 and 7.7. We show the excellent solution for this scheme. The numerical wiggles are obviously disappearing as we expect.

7.2 Momentum space CESE Method

7.2.1 Korteweg-de Vries equation

The KdV Eq. (4.2) has a solitonic solution

$$u(x,t) = -\frac{c}{2}\sec h^2(\frac{\sqrt{c}}{2}(x - ct + x_0)). \tag{7.7}$$

Note that the solution depends on speed c of soliton. So, multiply the solution by an arbitrary constant is no longer a solution. This invalidity of superposition principle is a notable property of nonlinear equation. Without loss of generality, we set the initial peak position at $x_0 = 0$. The wave propagates at speed c to the right of x-axis without shape change. The exact solution in momentum space is

$$u_e(p,t) = -p\csc h(\frac{\pi p}{\sqrt{c}})\exp(-ipct). \tag{7.8}$$

Figure 7.9 and Figure 7.10 depict the real and the imaginary part of the numerical results together with the analytic results at time $t = 5$. We arrive excellent agreements between the momentum space CESE calculation and the analytic results.

In Figure 7.11, the comparison of magnitude for the calculated and exact solutions at $t = 5$ with $c = 1$ is shown. For the soliton solution, though the real part and the imaginary part are both oscillating with time, but the magnitude is stationary as seen from Eq. (7.8). In Table 7.1, we listed the errors with respect to the grid size $\triangle p$. We plot in Figure 7.8 the error versus $\triangle p^2$. From the plot, the straight line shows that the error behaves in $\backsim O(\triangle p^2)$. This is the general scaling behavior of our developed momentum space CESE core scheme method.

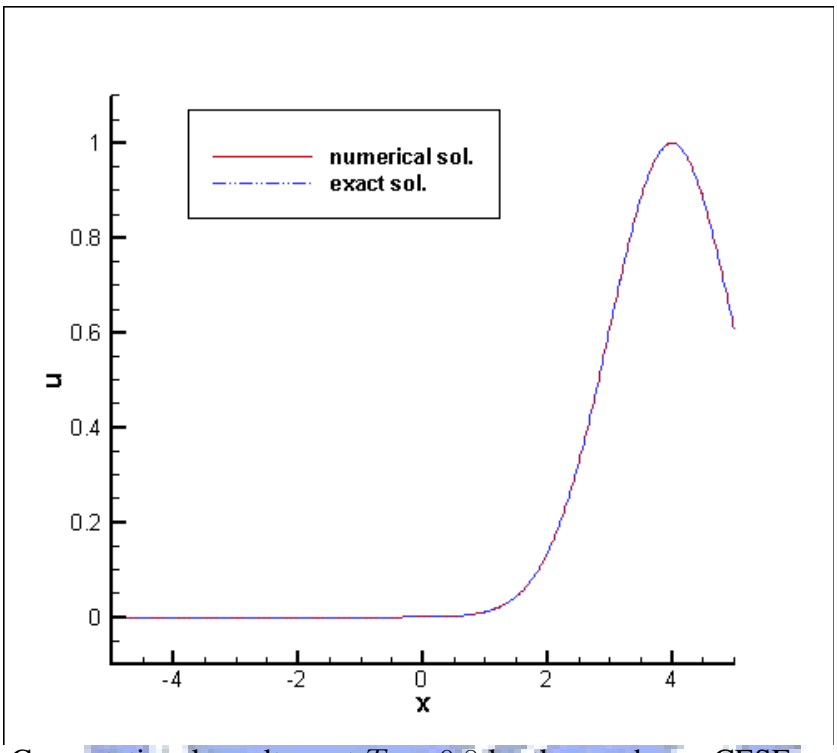

Figure 7.1: Computational results u at $T \approx 0.8$ by the a-scheme CESE method. Data obtained with $p \in [-5, 5]$, $\triangle p = 0.01$ and $\triangle t = 0.0005$.

Table 7.1: The root-mean-square error versus mesh size shows second-order behavior for KdV equation in our momentum space CESE method.

K: grid numbers; n: time steps	Mesh size	Error in momentum space
K: 26; n: 500	0.4	5.57E-02
K: 51; n: 500	0.2	1.23E-02
K: 101; n: 500	0.1	2.94E-03
K: 201; n: 1000	0.05	7.18E-04
K: 401; n: 2000	0.025	1.72E-04
K: 801; n: 4000	0.0125	3.57E-05

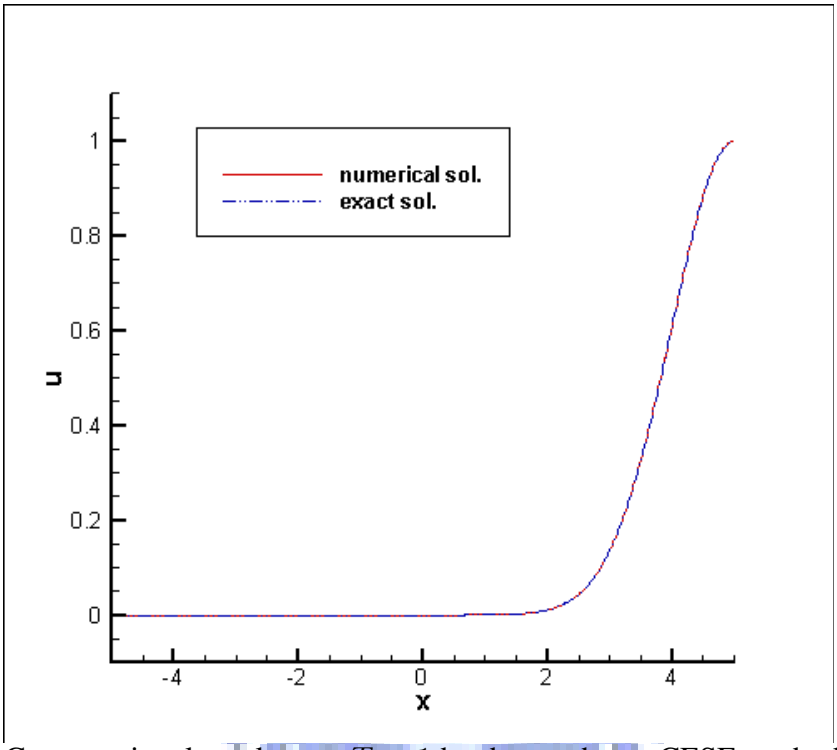

Figure 7.2: Computational results u at $T \approx 1$ by the a-scheme CESE method. Data obtained with $p \in [-5, 5]$, $\triangle p = 0.01$ and $\triangle t = 0.0005$.

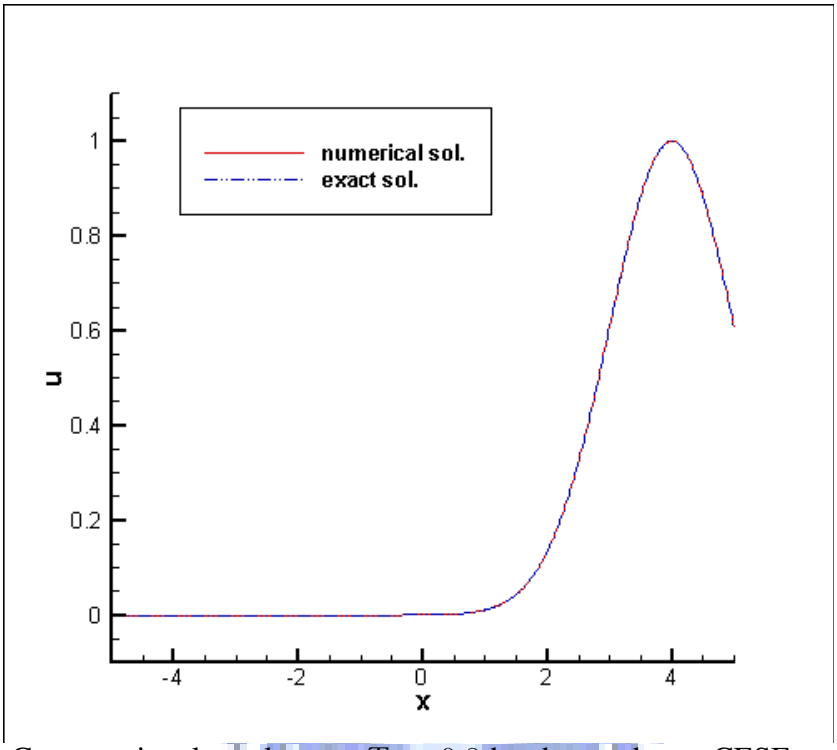

Figure 7.3: Computational results u at $T \approx 0.8$ by the c-scheme CESE method. Data obtained with $p \in [-5, 5]$, $\triangle p = 0.01$ and $\triangle t = 0.0005$.

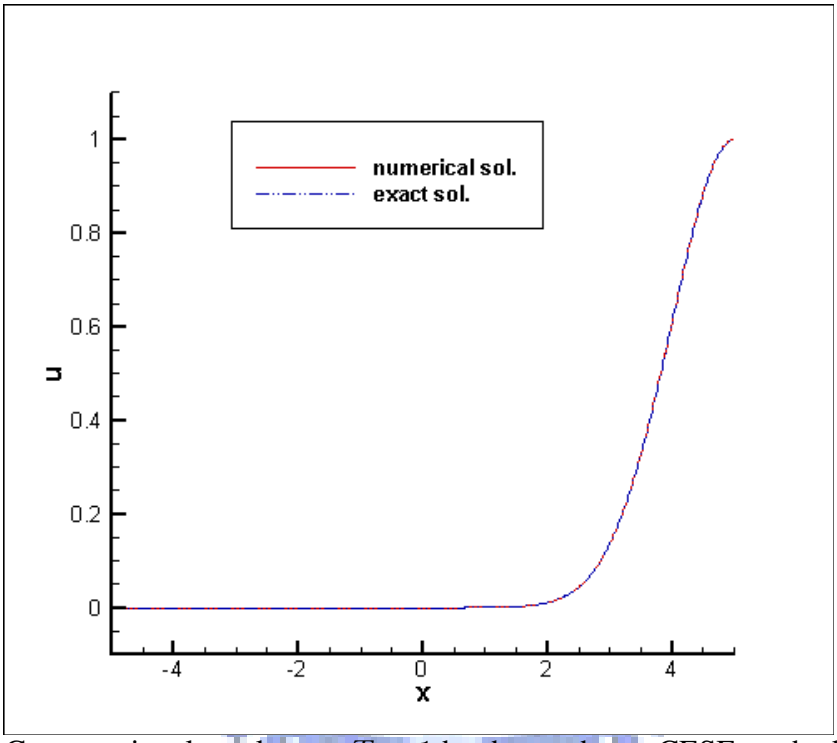

Figure 7.4: Computational results u at $T \approx 1$ by the c-scheme CESE method. Data obtained with $p \in [-5, 5]$, $\triangle p = 0.01$ and $\triangle t = 0.0005$.

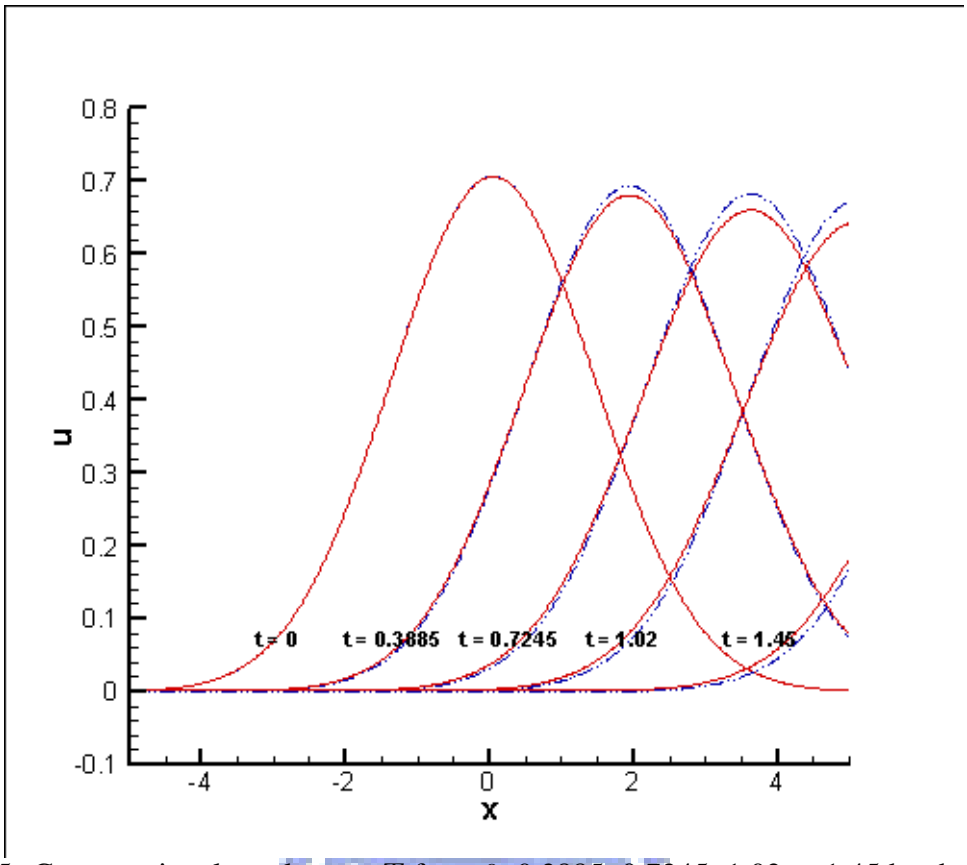

Figure 7.5: Computational results u at T from 0, 0.3885, 0.7245, 1.02 to 1.45 by the a-μ scheme CESE method. Data obtained with $p \in [-5, 5]$, $\triangle p = 0.01$ and $\triangle t = 0.0005$. DashDotDot line: exact solution. Solid line: numerical solution.

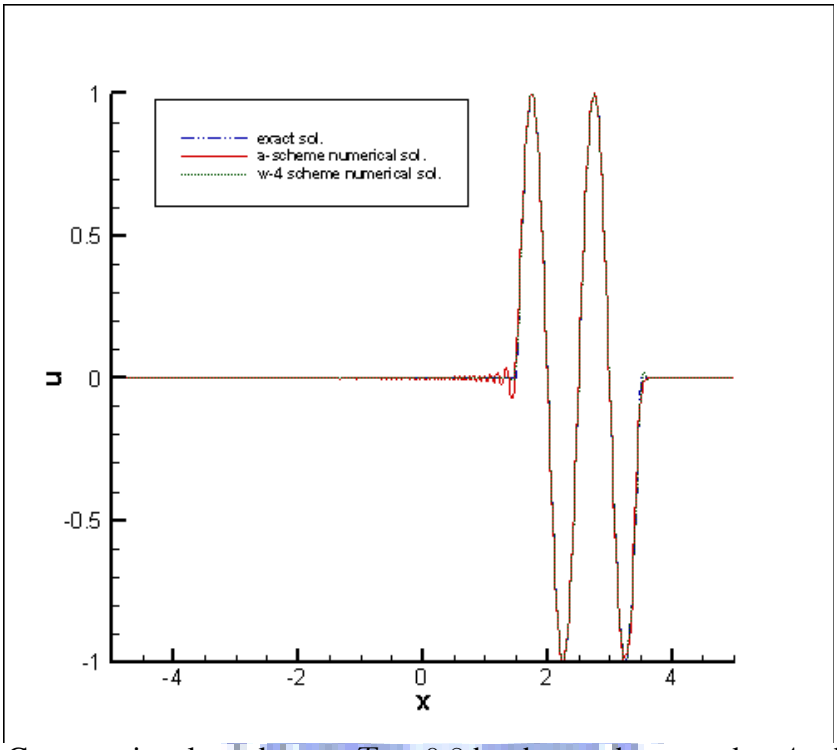

Figure 7.6: Computational results u at $T \approx 0.8$ by the a-scheme and w-4 scheme CESE method. Data obtained with $p \in [-5, 5]$, $\triangle p = 0.01$ and $\triangle t = 0.0005$.

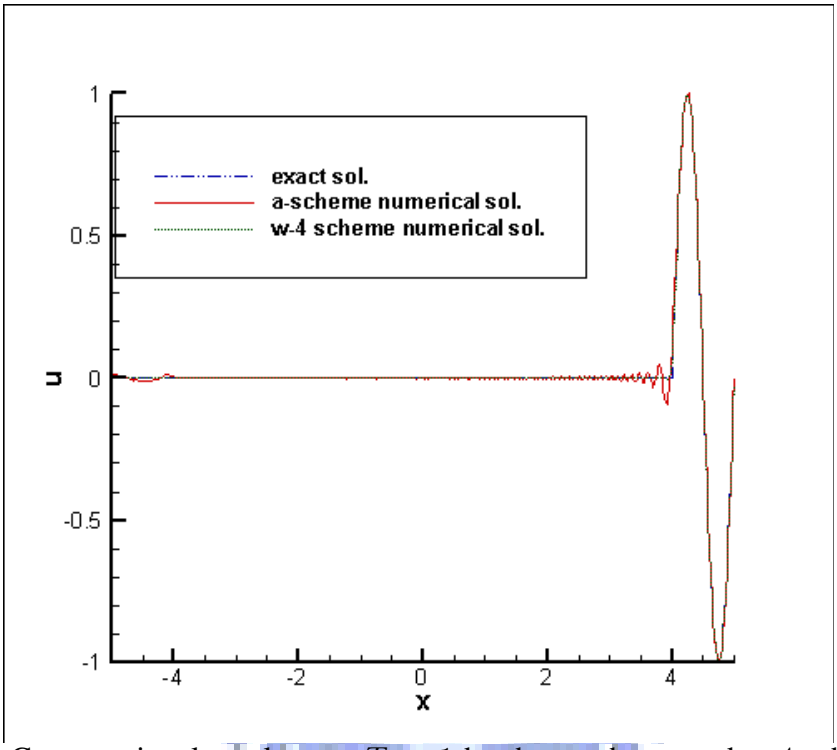

Figure 7.7: Computational results u at $T \approx 1$ by the a-scheme and w-4 scheme CESE method. Data obtained with $p \in [-5, 5]$, $\triangle p = 0.01$ and $\triangle t = 0.0005$.

7.2.2 Burgers's equation

Let

$$\begin{aligned} V &= \frac{1}{2}\left(u(-\infty)+u(\infty)\right), \\ D &= \frac{1}{2}\left(u(-\infty)-u(\infty)\right). \end{aligned} \tag{7.9}$$

The exact solution of the Burgers's equation Eq. (4.11) is

$$u(x,t) = V - D\tanh\left[\frac{V(x-Vt)}{2\upsilon}\right]. \tag{7.10}$$

We may set $u(\infty)=0$, then the exact solution becomes

$$u(x,t) = V - V\tanh\left[\frac{V(x-Vt)}{2\upsilon}\right]. \tag{7.11}$$

Where $V = \frac{1}{2}u(-\infty) > 0$ and $D = \frac{1}{2}u(-\infty) = V$. The corresponding exact solution in momentum space is

$$u(p,t) = \begin{cases} V\delta(p) & , \text{ for } p=0 \\ i\upsilon\exp(-ipVt)\operatorname{csc}h(\frac{\upsilon\pi p}{V}), & \text{for } p\neq 0 \end{cases} \tag{7.12}$$

where $\delta(p)$ is delta function. The parameters here we use are $V=1$ and $\upsilon=1$. Because of the infinite value can't show in the figures. The delta function of the analytic solution we plot in the figures is just set as a finite value. Figure 7.12 and Figure 7.14 depict the real and the imaginary part of the numerical results together with the analytic results at time $t=5$. For describing the shock behavior of Burgers's equation in detail Figure 7.13 shows the zoom up of figure 7.12 near the shock, and Figure 7.15 shows zoom up of Figure 7.14. We arrive excellent agreements between the momentum space CESE calculation and the analytic results. The momentum space CESE method obtained the accurate solution when the shock is occurred. This is the same capability as coordinate space CESE method.

In the chapter 5, we introduce the non-uniform grid Momentum Space CESE Method. The purpose is to generate the grids which are much denser in center. The Burgers's equation Eq. (4.11) has a shock in the center of the space domain. The dense grid in center is especially

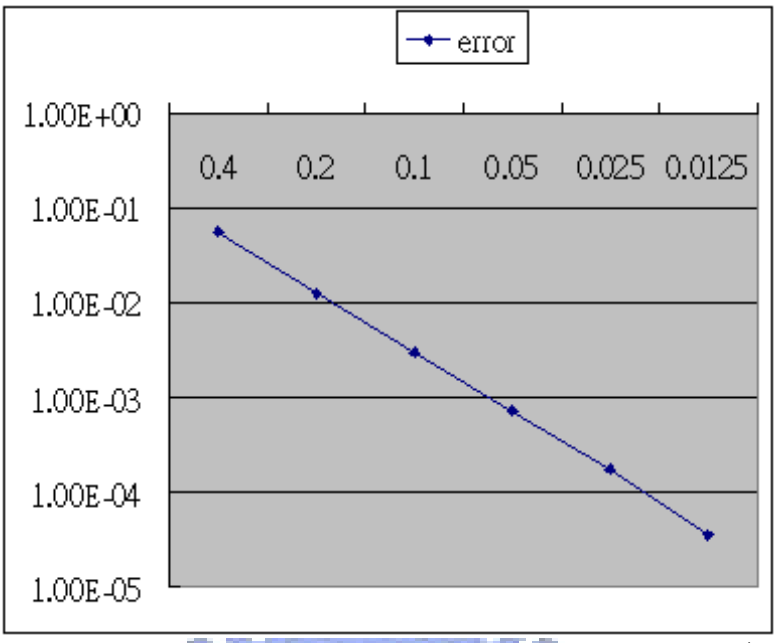

Figure 7.8: Error in momentum space as function of square of grid size $\triangle p$. It shows $O(\triangle p^2)$ behavior.

useful for this problem. The goal is to obtain the accurate solution but ease the computational time. Because of efficient grid is used the less grid points can obtain the similar accuracy. We compare the non-uniform grid momentum space CESE method without transform and with the two different transform. Figure 7.16, 7.17 is the nonuniform grid method without any transform, Figure 7.18, 7.19 is the nonuniform grid method with the transform as Eq. (5.24), and Figure 7.20, 7.21 is the nonuniform grid method with the transform as Eq. (5.25). The above figures shows the non-uniform grid method arrive excellent agreements in the less grid points. The grid points are 500 for the each case. The transform cases have improved the implementation time. And the similar accuracy is obtained. It shows the importance of the transform when the further implementation of higher-dimensional question.

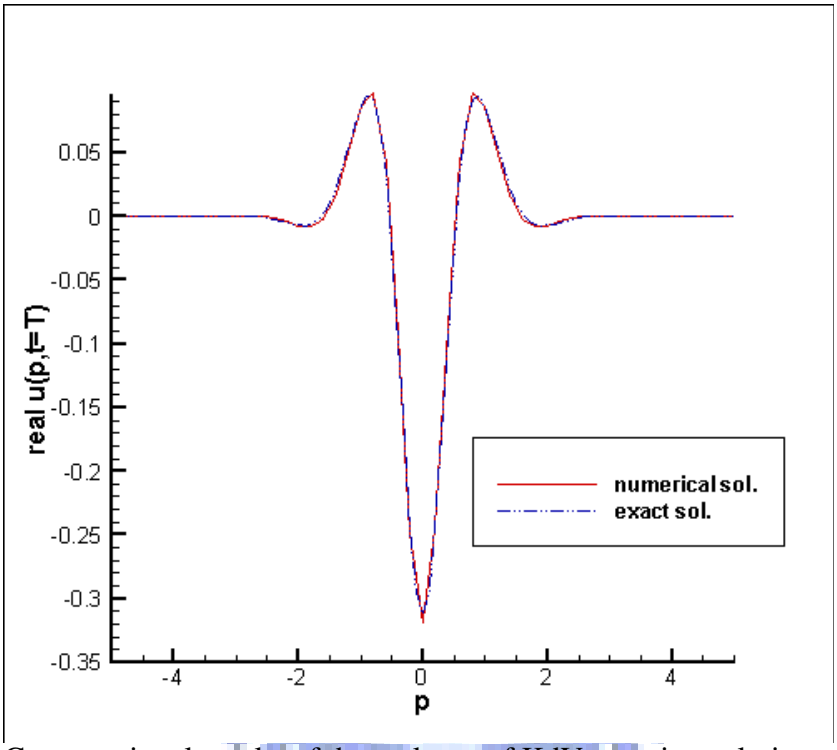

Figure 7.9: Computational results of the real part of KdV equation solution at $t = 5$ obtained with $p \in [-5, 5]$ and $\triangle t = 0.01$.

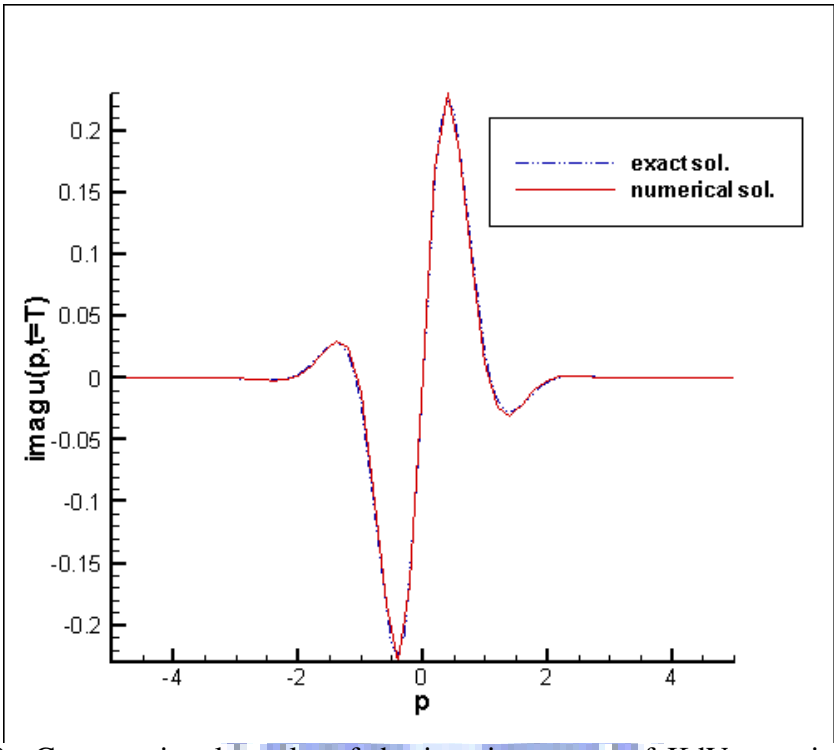

Figure 7.10: Computational results of the imaginary part of KdV equation solution at $t = 5$ obtained with $p \in [-5, 5]$ and $\triangle t = 0.01$.

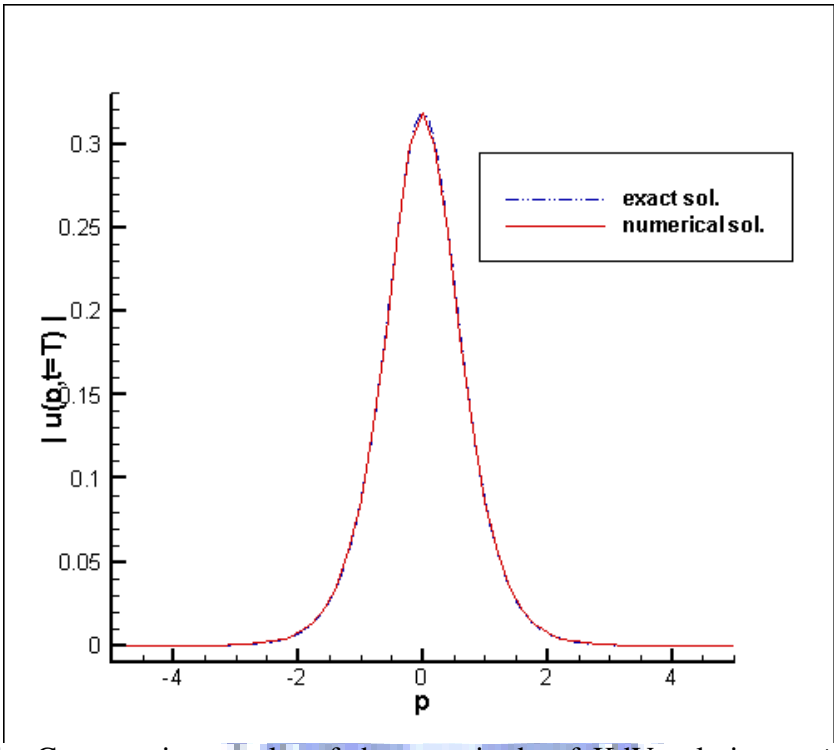

Figure 7.11: Computation results of the magnitude of KdV solution at $t = 5$ obtained with $p \in [-5, 5]$ and $\triangle t = 0.01$.

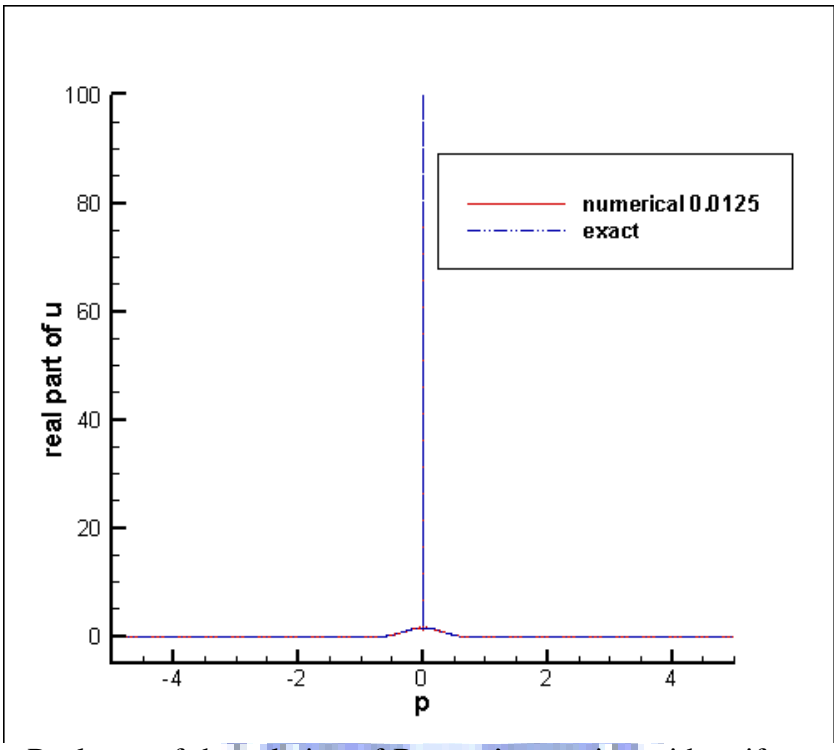

Figure 7.12: Real part of the solution of Burgers's equation with uniform grid ($\triangle x = 0.0125$). $V = 1, \upsilon = 1$ and simulation time is 5.

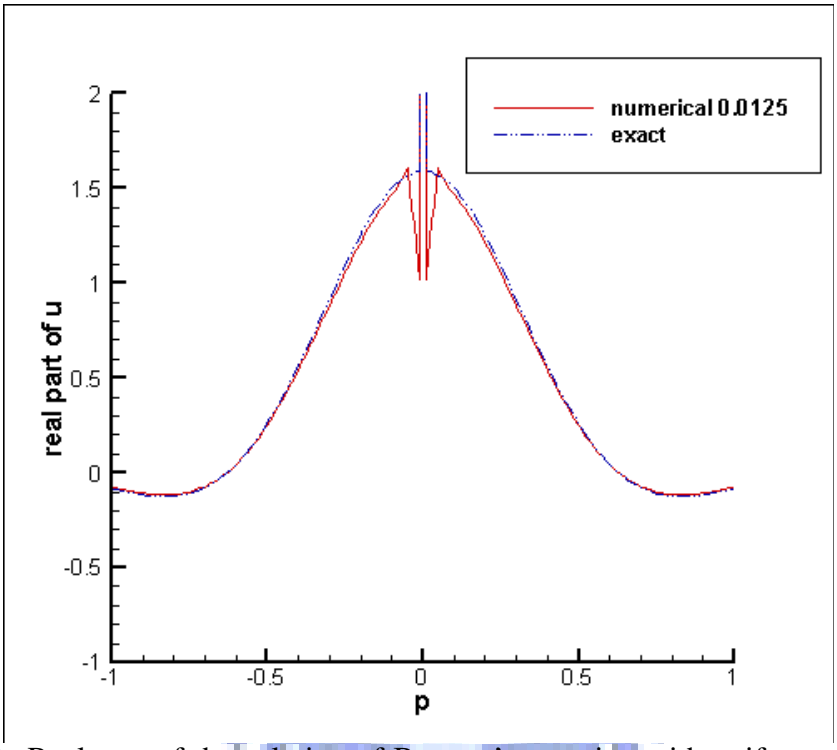

Figure 7.13: Real part of the solution of Burgers's equation with uniform grid ($\triangle x = 0.0125$). $V = 1, \upsilon = 1$ and simulation time is 5. (locate the view to center)

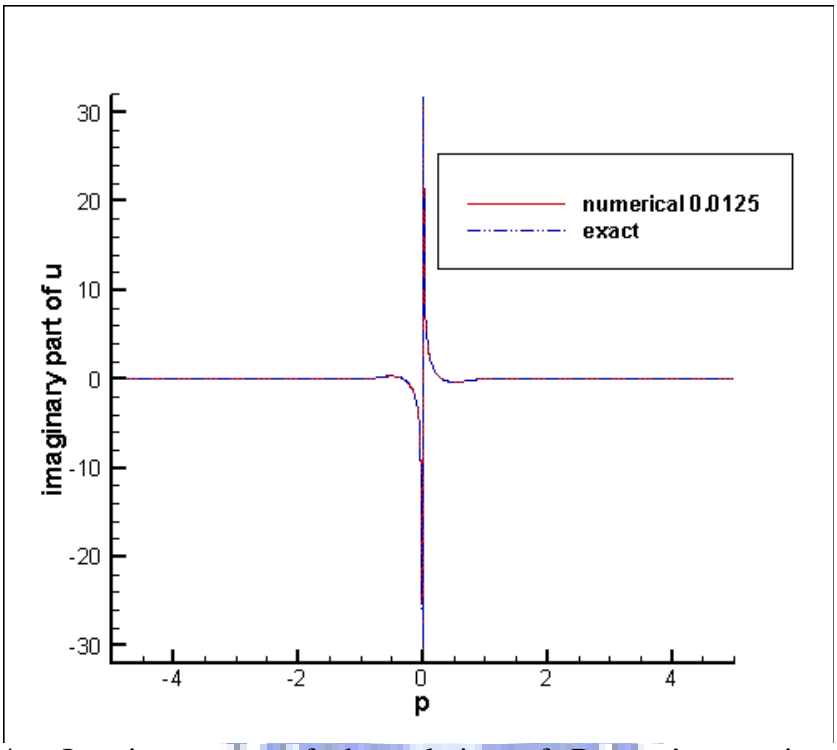

Figure 7.14: Imaginary part of the solution of Burgers's equation with uniform grid ($\triangle x = 0.0125$). $V = 1, \upsilon = 1$ and simulation time is 5.

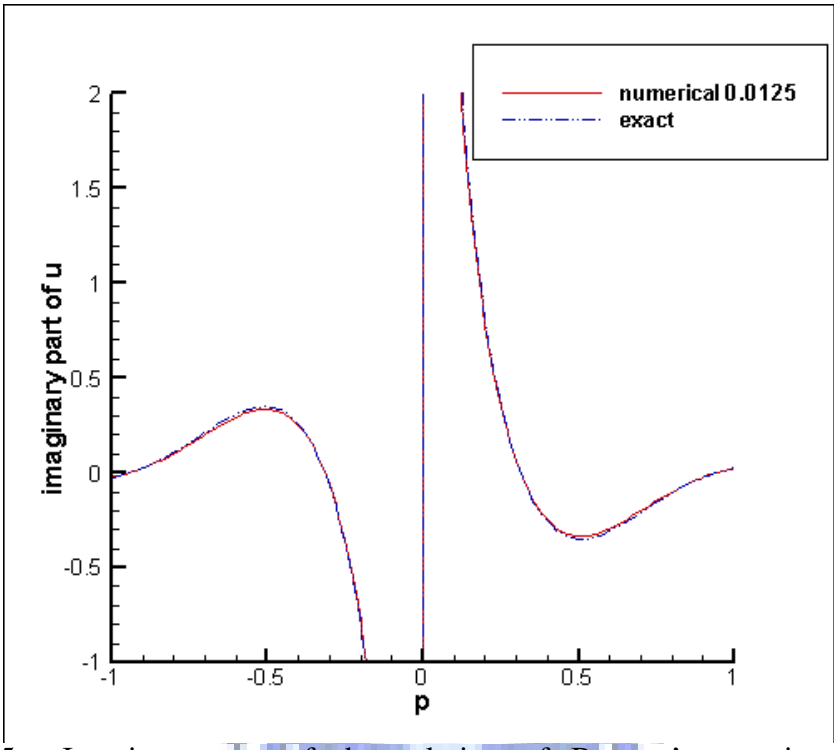

Figure 7.15: Imaginary part of the solution of Burgers's equation with uniform grid ($\triangle x = 0.0125$). $V = 1, \upsilon = 1$ and simulation time is 5. (locate the view to center)

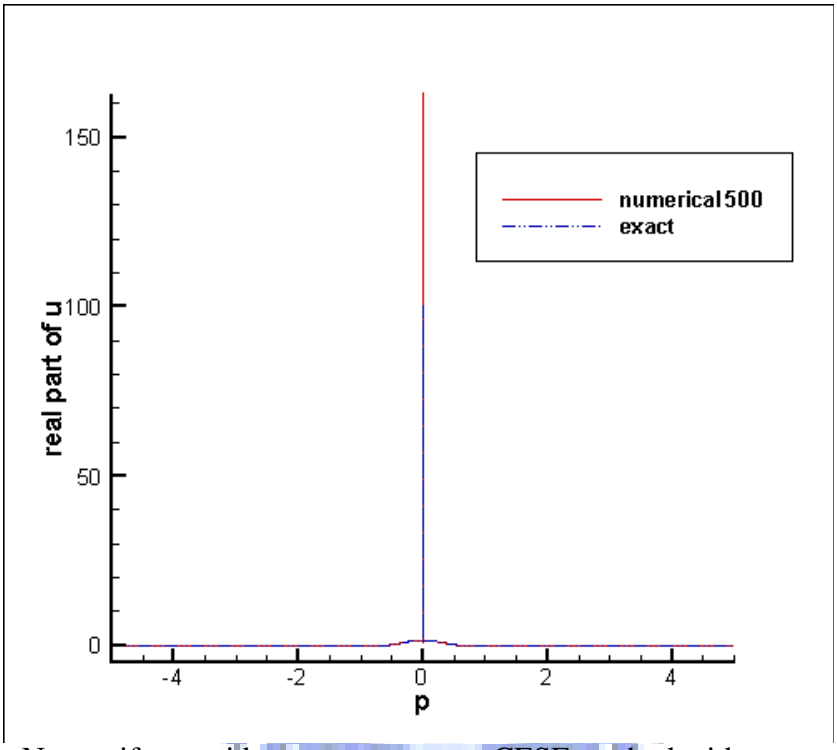

Figure 7.16: Non-uniform grid momentum space CESE method without any transformation. The real part solution of Burgers's equation is presented.

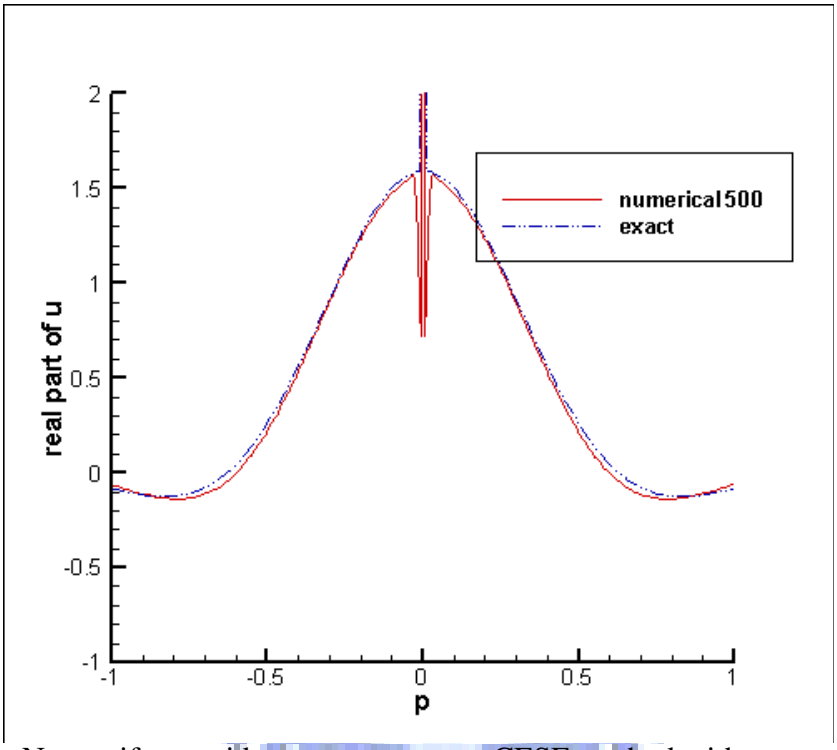

Figure 7.17: Non-uniform grid momentum space CESE method without any transformation. The real part solution of Burgers's equation is presented. (locate the view to center)

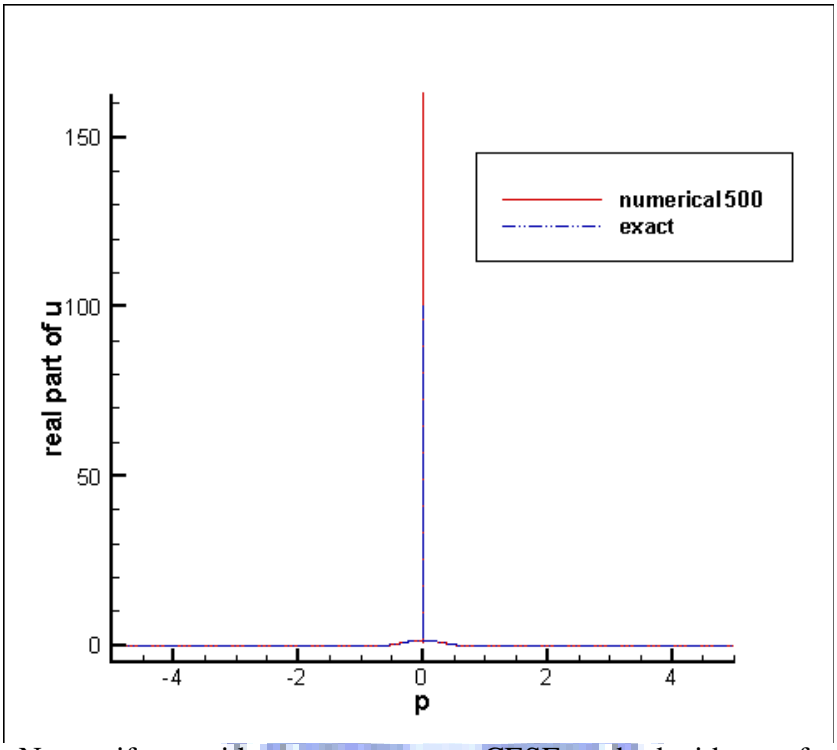

Figure 7.18: Non-uniform grid momentum space CESE method with transformation as Eq. (5.21). The real part solution of Burgers's equation is presented.

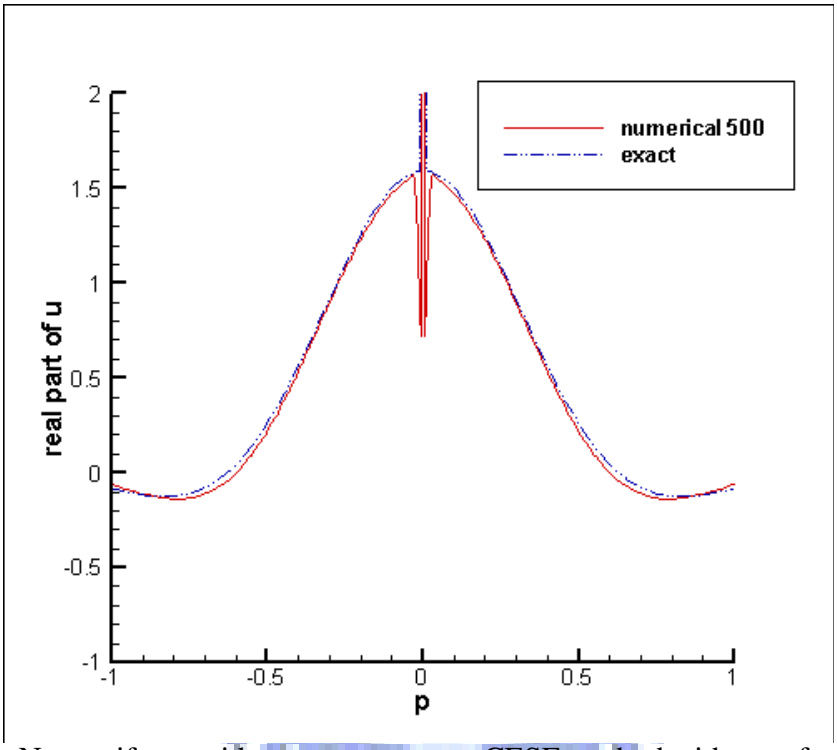

Figure 7.19: Non-uniform grid momentum space CESE method with transformation as Eq. (5.21). The real part solution of Burgers's equation is presented. (locate the view to center)

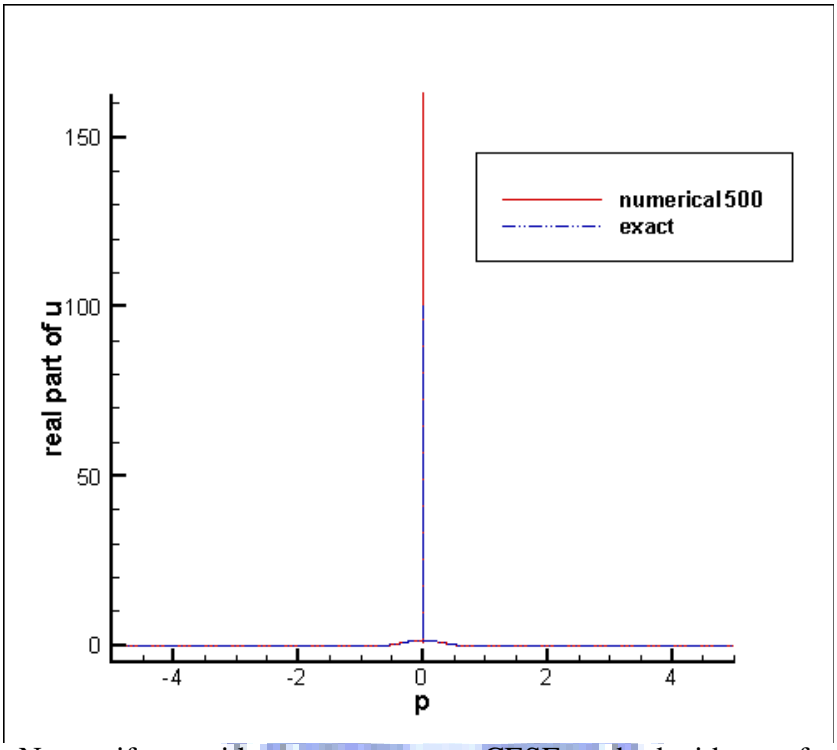

Figure 7.20: Non-uniform grid momentum space CESE method with transformation as Eq. (5.22). The real part solution of Burgers's equation is presented.

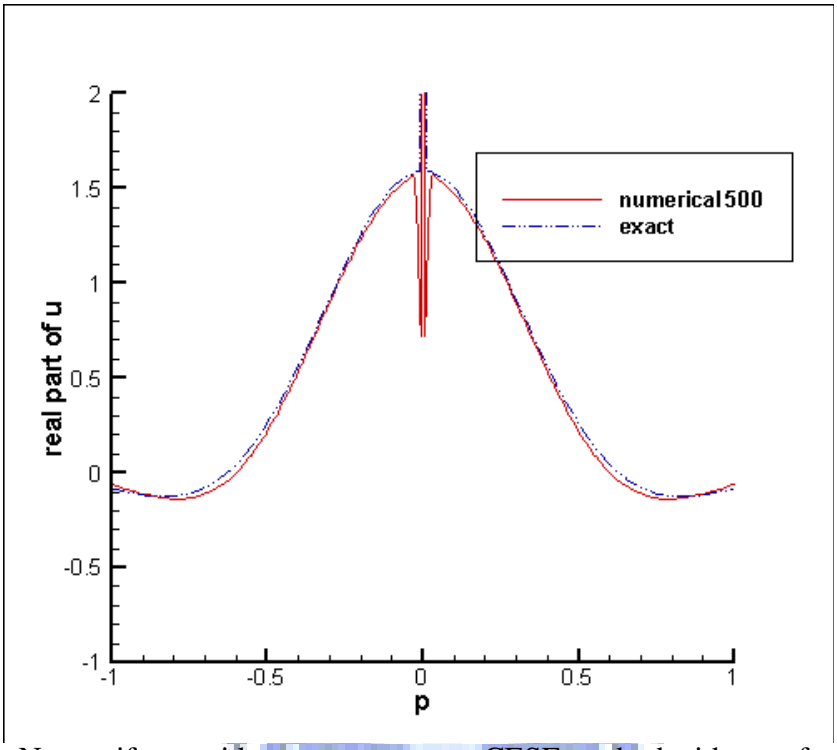

Figure 7.21: Non-uniform grid momentum space CESE method with transformation as Eq. (5.22). The real part solution of Burgers's equation is presented. (locate the view to center)

Chapter 8 Numerical results for Quantum Mechanical Problem

In order to model the response of an atomic electron, we have used the so-called "soft-Coulomb" potential defined in Eq. (6.2). With c =1.41, the ground-state energy is the same as for Ar atoms: $\epsilon_0 = -0.58$ a.u. [13]. This class of potentials has been shown to be useful to reproduce the main features of laser-atom interactions in the strong-field regime, for linearly polarized laser. The smaller ten bound state energies for our computation are list as table 8.1. Examples for the ATI spectra, simulate when the above system is submitted to a sinusoidal shape laser pulse with frequency $\omega = 0.0577$ a.u. ≈ 1.57 eV, with total duration of 9 cycles, are shown in Figure 8.1, 8.2 and 8.3. The Figure 8.4 conbine all of the different intensities to one figure, but only plot the first degenerate state. The spectra are deduced from the spectral analysis of the final wave function obtained by solving the Eq. (6.1). Typical values for the grid spacing is $\triangle p = 0.01$, $\triangle t = 0.0019$, and the size of the box is [-5,5]. We have checked that our results are robout while varying these parameters. In Figure 8.5, the ATI spectra for three selected intensities are shown. One can check that, at $E_m = 1.12 \times 10^{14}\ Wcm^{-2}$, a conspicuous enhancement shows up in the region comprised between $7Up$ and $10Up$. Conversely, it almost disapears at the neighboring intensities $E_m = 1.02 \times 10^{14}\ Wcm^{-2}$ and $E_m = 1.22 \times 10^{14}\ Wcm^{-2}$. In spite of the fact that the bare state basis is not really adequate for analyzing the time-dependent wave function of the atom "dressed" by the external field, it can provide useful indications on the population dynamics. With this caveat in mind, the results of Figure 8.6 confirm the existence of an important transfer of population in excited state $n = 3$ at the intensity when the enhancement is observed.

Table 8.1: List the bound state energies (state: energy (a.u.)). (i) Domain = (-5,5), (ii) Grid numbers = 1024.

1: -0.579551339149484	2: -0.253565788269046
3: -0.142360016703607	4: -8.848649263382038E-002
5: -6.089104339480454E-002	6: -4.384820908308049E-002
7: -3.334389254450847E-002	8: -2.595771290361919E-002
9: -2.091300487518327E-002	10: -1.707826927304287E-002

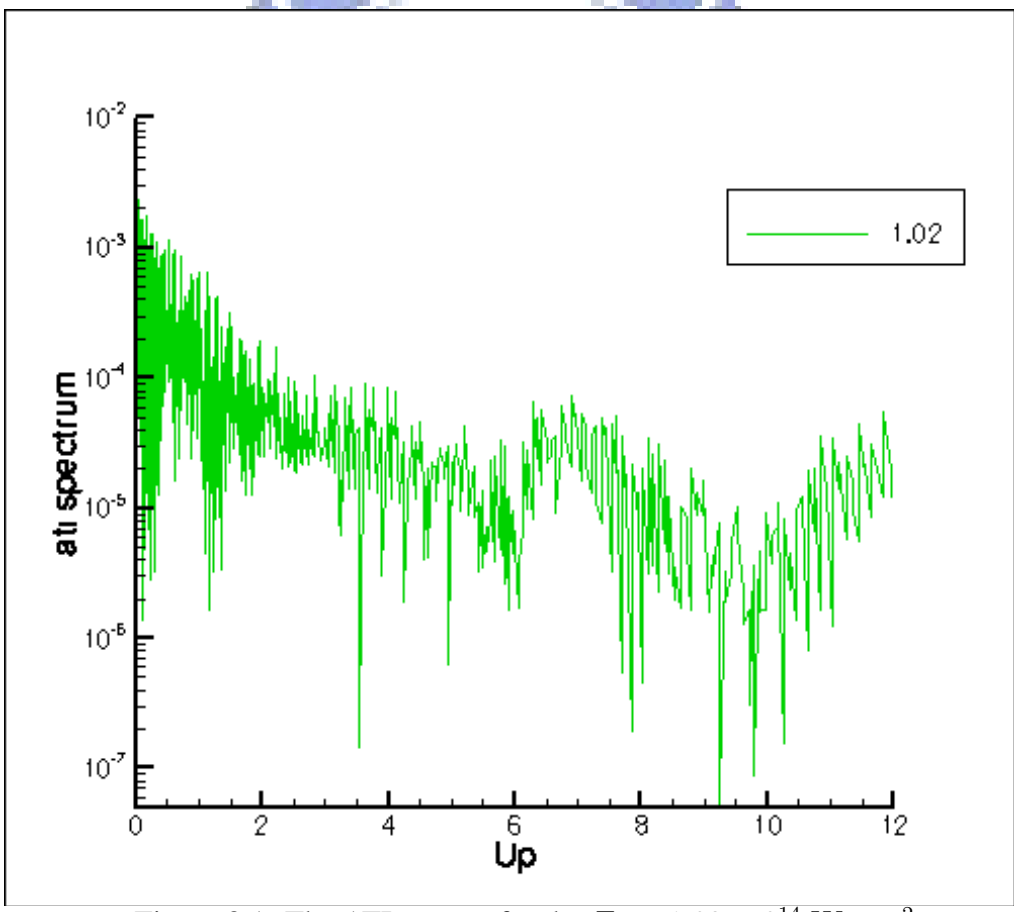

Figure 8.1: The ATI spectra for the $E_0 = 1.02 \times 0^{14}\ Wcm^{-2}$.

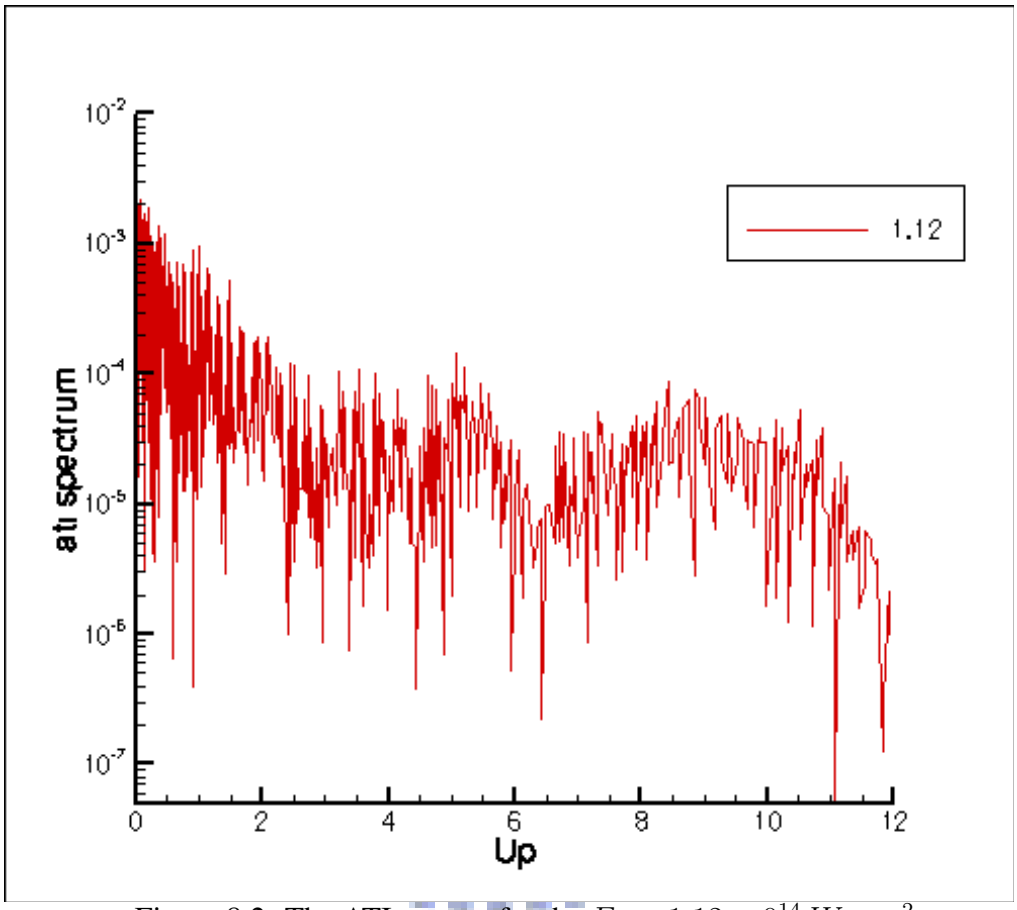

Figure 8.2: The ATI spectra for the $E_0 = 1.12 \times 0^{14}\, W cm^{-2}$.

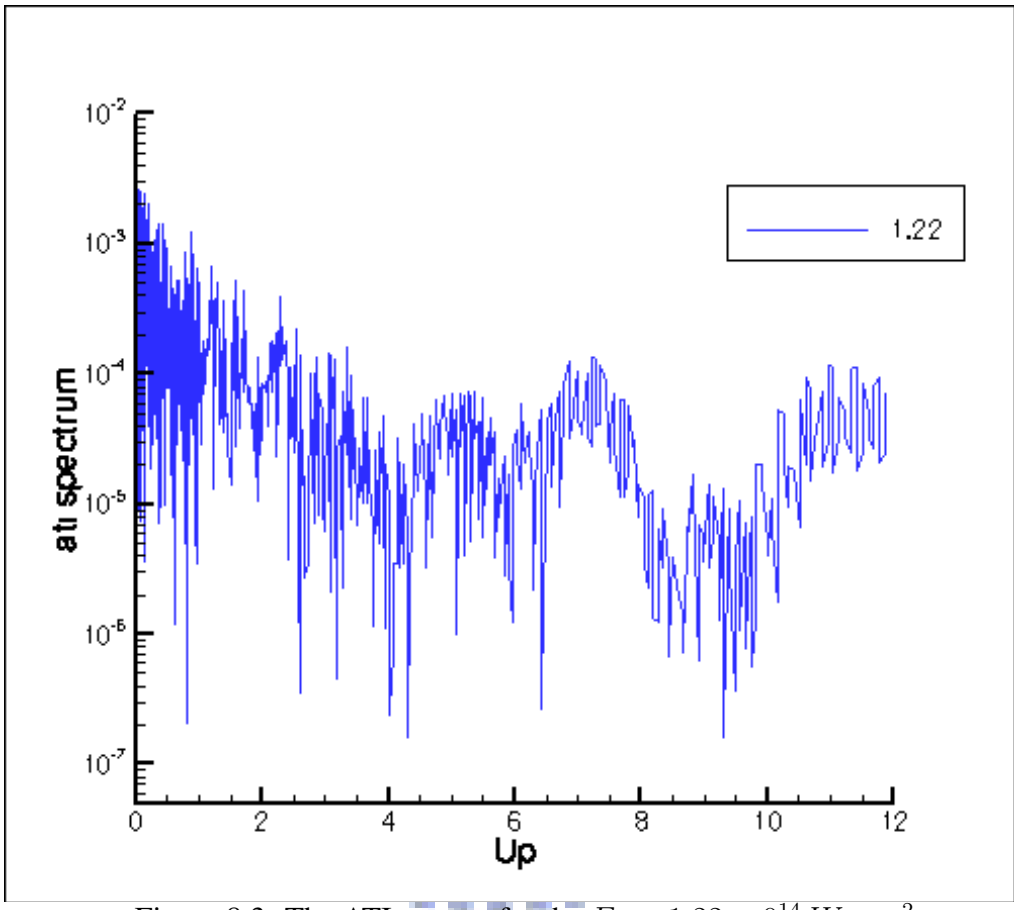

Figure 8.3: The ATI spectra for the $E_0 = 1.22 \times 0^{14}\, Wcm^{-2}$.

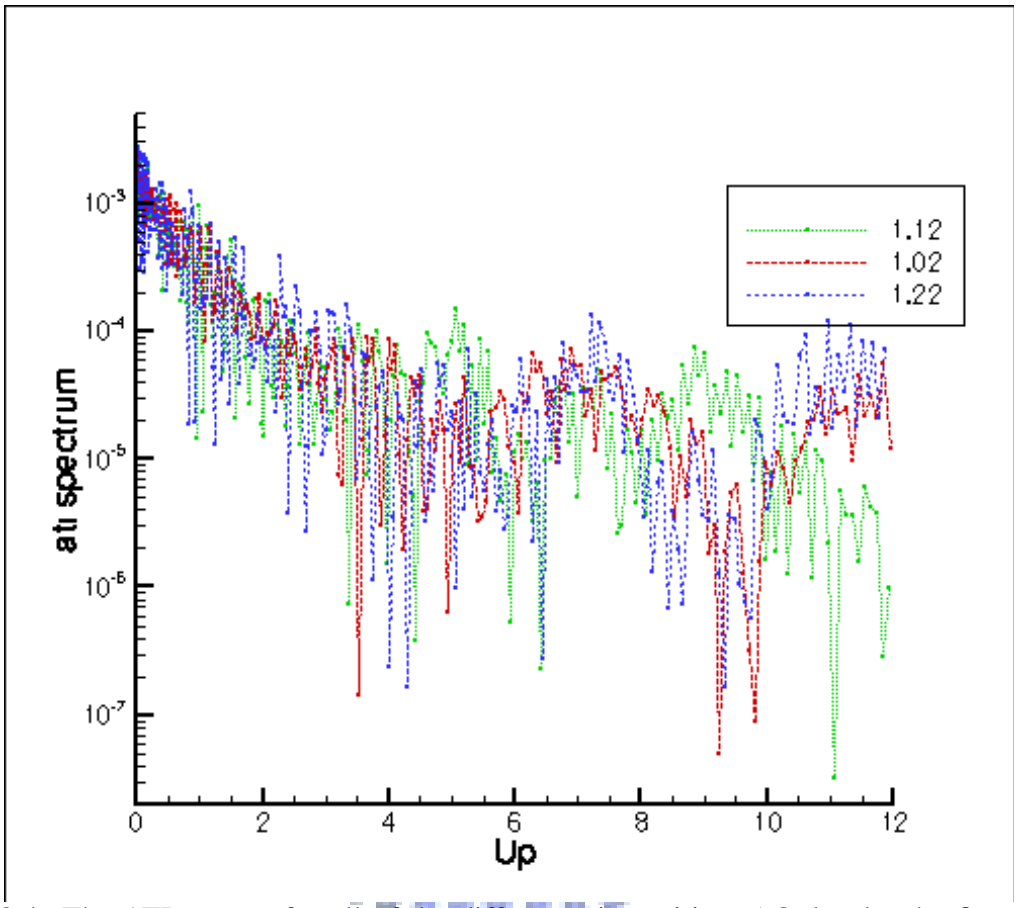

Figure 8.4: The ATI spectra for all of the difference intensities. (Only plot the first degenerate state)

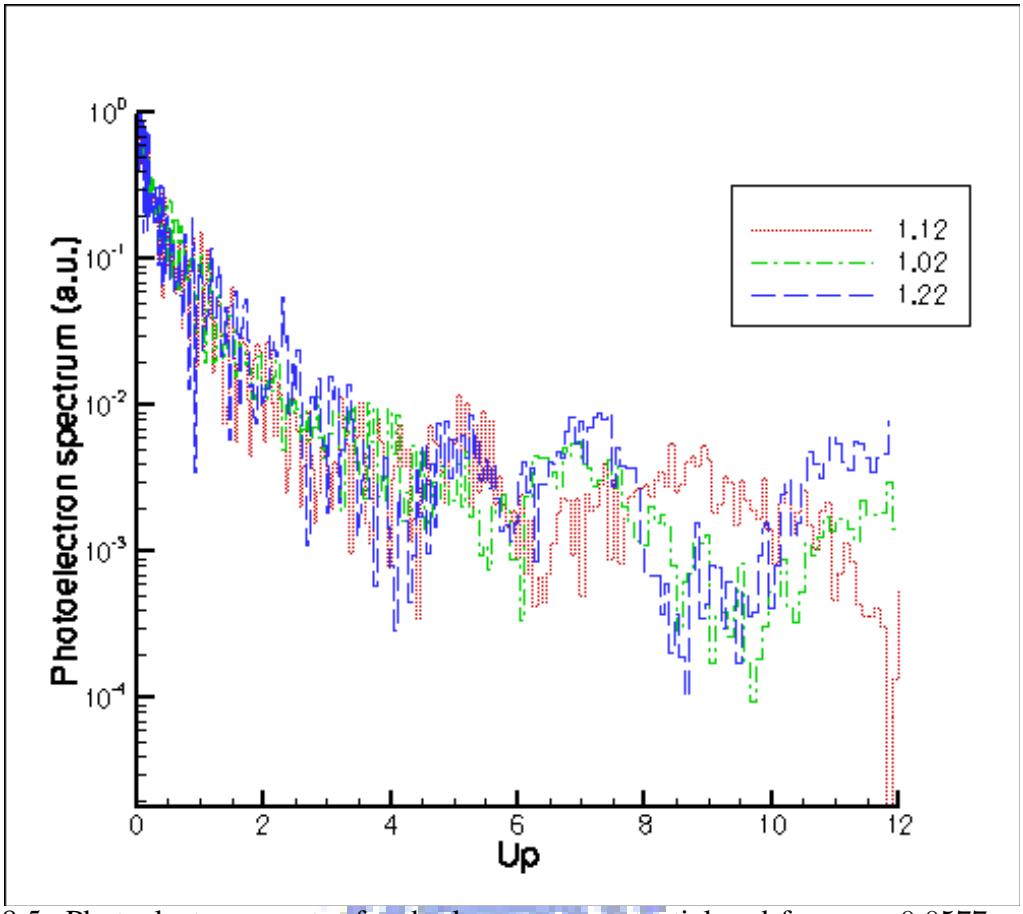

Figure 8.5: Photoelectron spectra for the long-range potential and for $\omega = 0.0577$ a.u. Dotted, DashDot, LongDash correspond to intensities of $1.12 \times 10^{14}\ Wcm^{-2}$, $1.02 \times 10^{14}\ Wcm^{-2}$ and $1.22 \times 10^{14}\ Wcm^{-2}$, respectively. The pulse duration is $9T_L$.

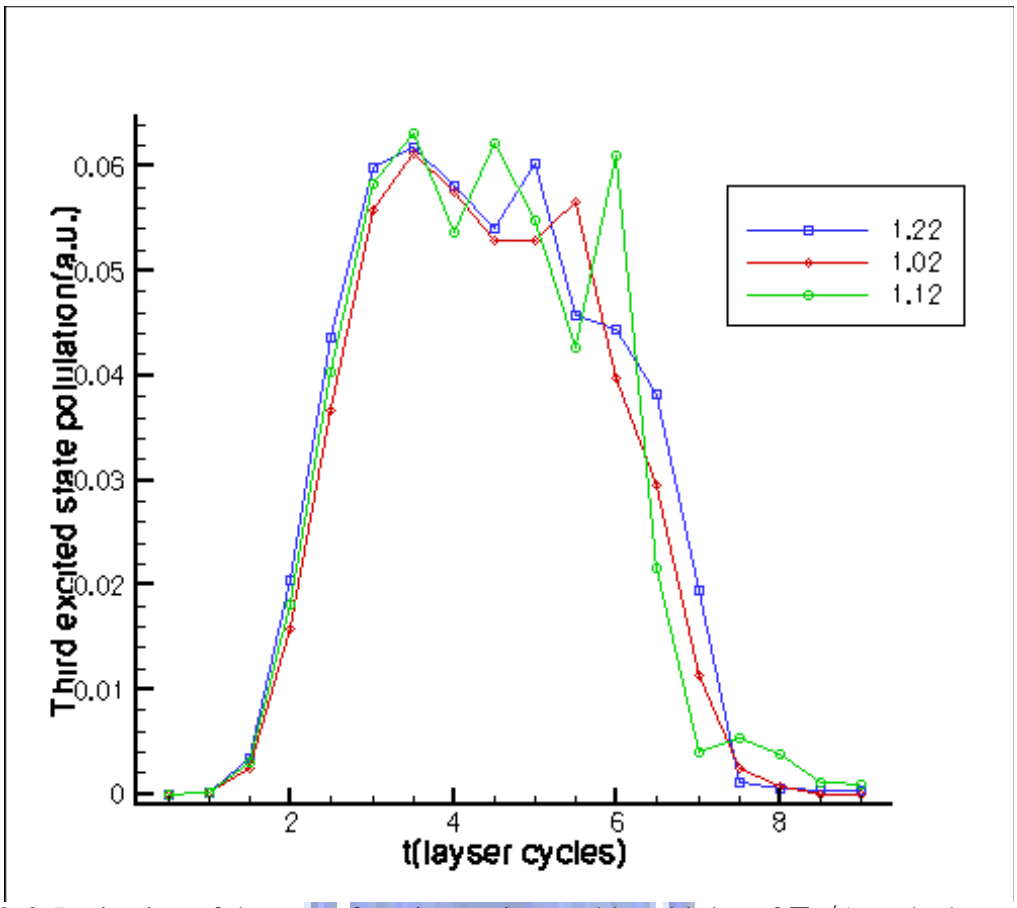

Figure 8.6: Projection of the wave function at times odd multiples of $T_L/4$ on the bare state $n = 3$ for three different intensities. Diamond, Circle and Square correspond to intensities of 1.02×10^{14} Wcm^{-2}, 1.12×10^{14} Wcm^{-2}(when the enhancement is observed) and 1.22×10^{14} Wcm^{-2}, respectively.

Chapter 9 Discussion and conclusions

In this thesis, we develop the CESE method in momentum space. We investigate the basic one-dimensional wave equation, convection equation, convection-diffusion equation, nonlinear Korteweg-de Vries equation, shock wave Burgers's equation and a quantum mechanical problem. The scope is on the fundamental part. In each problem, the momentum space CESE core scheme is developed for an explicit time-marching scheme. It is straightforward for linear problems. While for nonlinear problem such as KdV equation and Burgers's equation the convolution integral of the unknown functions in the source term is involved. We employ the half-step grid size for the convolutions and the iterations in each half-time marching step for the nonlinearity. Above method we has introduced is sufficient only to uniform grid problem. For non-uniform grid problem, it is not solved. We finally figure out the idea of the solution element must be introduced as suitable modification. The troubles occur in convolution integral for nonlinear problems is conquered by a consistent treatment. When numerical grid is not on the node points, it is just expanded as a Taylor expansion from the nearly solution element. For the non-reflecting boundary condition, the zero boundary condition and the ghost cell method is employed. It shows that the ghost cell method is excellent in coordinate and momentum space, even when the domain size is small. Because of the boundary value is sufficiently small in momentum space. It is enough to use the zero boundary condition. For non-uniform grid momentum space CESE method, we introduce a transformation method to shorter the computational time and improve the convolution integral accuracy. The importance of this approach for higher-dimensional problems will be investigated in our future studies. We calibrate each system with known exact solution. We have shown that the momentum space CESE method works well for the systems from classical wave equation, nonlinear equation to quantum mechanical problem. And the error behavior of the developed

scheme is second-order. Strictly speaking, the method used in this work is not regular core scheme. But it is still capable of generating highly accurate solution by using only the concept of flux conservation and simple approximation techniques. The main advantages for the momentum space CESE method, compared to the traditional CESE method in coordinate space are twofold. First, the boundary conditions are fulfilled automatically. That is, for sufficient large momentum value, the function and its derivatives are simply vanishing at the numerical boundary. This is because the kinetic energy of a system is physically finite. Second, the information of the wave is preserved completely inside the numerical momentum region without flowing out from the boundary like the coordinate space method. This will be especially useful in treating scattering problems in the future.With the efficient momentum space CESE method, we are able to calculate the ATI photoelectron spectra. We elucidate the capability of this method with the atom either under a very high intensity or a very long duration laser pulse to show the nice features. There is no loss of the continuous part of the wave functions, unlike filtering function employed in coordinate space method to prevent boundary reflection. In this simulation, the conspicuous enhancements appear in the high-energy part of the above-threshold (ATI) spectra, too. Because no information of wave is lost. Comparing with experiment data, the high-energy part ATI spectra obtained from our method is more accurate than the method from other coordinate space method. Further applications of the method to intense laser pulses on atoms and molecules will be presented in the future. In the future, we will develop the higher order of accuracy, and the higher dimensional momentum space CESE method to practical useful in solving realistic time-dependent problems.

References (or Bibliography)

[1]. S.C. Chang and W.M. To, *"A New Numerical Framework for Solving Conservation Laws – The Method of Space-Time Conservation Element and Solution Element,"* NASA/TM 104495 (1991), J. Comput. Physics, 119, 295 (1995).

[2]. X.-Y. Wang, C.-Y. Chow and S.C. Chang, *"Application of the Space-Time Conservation Element and Solution Element Method to One-Dimensional Advection-Diffusion Problems,"* NASA/TM 209068 (1999).

[3]. S.-C. Chang, A. Himansu, C.-Y. Loh, X.-Y. Wang and S.-T.J. Yu, *"Robust and Simple Non-Reflecting Boundary Conditions for the Euler Equations, A New Approach Based on the Space-Time CE/SE Method,"* NASA/TMX2003-212495/REV1 (2003).

[4]. S.C. Chang and X.Y. Wang, *"Multi-Dimensional Courant Number Insensitive CE/SE Euler Solvers for Applications Involving Highly Nonuniform Meshes,"* AIAA Paper (2003)-5285, presented at the 39th AIAA/ASME/SAE/ASEE Joint Propulsion Conference and Exhibit, July 20-23 (2003), Huntsville, AL.

[5]. S.C. Chang, *"Courant Number and Mach Number Insensitive CE/SE Euler Solvers,"* AIAA Paper (2005)-4355, presented at the 41th AIAA/ASME/SAE/ASEE Joint Propulsion Conference and Exhibit, July 11-13 (2005), Tucson, AZ.

[6]. S.C. Chang, *"On Space-Time Inversion Invariance And Its Relation To Non-dissipatedness Of a CESE Core Scheme,"* 42th AIAA Joint Propulsion Conference (2006).

[7]. S.C. Chang, *"The Space-Time CESE Method—motivating ideas, basic schemes and its recent developments,"* first Taiwan-USA workshop on CESE Method (2007).

[8]. More details and refferences can be found in http://www.grc.nassa.gov/WWW/microbus/.

[9]. C. Cohen-Tannoudji, J. Dupont-Roc, C. Fabre, and G. Grynberg, *"Comment on the Momentum-Translation Approximation,"* Phys. Rev. A8, 2747 (1973).

[10]. T.F. Jiang and S.-I. Chu, *"High-order harmonic generation in atomic hydrogen at 248 nm: Dipole-moment versus acceleration spectrum,"* Phys. Rev. A46, 7322 (1992).

[11]. U.L. Pen and T.F. Jiang, *"Strong-field effects of the one-dimensional hydrogen atom in momentum space,"* Phys. Rev. A46, 4297 (1992).

[12]. U.L. Pen and T.F. Jiang, *"Direct momentum-space calculations for the resonant multiphoton processes of a hydrogen atom under intense laser pulses,"* Phys. Rev. A53, 623 (1996).

[13]. Joseph Wassaf, Valerie Veniard, Richard Taieb, Alfred Maquet, *"Roles of resonances and recollisions in strong-field atomic phenomena: Above-threshold ionization,"* Phys. Rev. A 67, (2003).

[14]. Joseph Wassaf, Valerie Veniard, Richard Taieb, Alfred Maquet, *"Strong Field Atomic Ioniza-*

tion: Origin of High-Energy Structures in Photoelectron Spectra," Phys. Rev. Letters (2003).

[15]. T.F. Jiang, *"Calculation of atomic hydrogen and its photoelectron spectra in momentum space,"* Comp. Phys. Commun. 178, 571 (2008).

[16]. P.G. Drazin and R.S. Johnson, *"Solitons : an Introduction,"* (Cambridge Univ. Press, Cambridge, 1989).

[17]. G.B. Arfken and H.J. Weber, *"Mathematical Method for Physicists,"* 4th Ed. (Academic Press, San Diego, 1995).

[18]. Zhaojun Bai, James Demmel, Jack Dongarra, Axel Ruhe and Henk van der Vorst, editors. *"Templates for the Solution of Algebraic Eigenvalue Problems : A Practical Guide,"* SIAM, Philadelphia, (2000).

[19]. J.H. Mathews and K.D. Fink, *"Numerical Methods Using Matlab,"* 4th Ed. (Pearson Prentice Hall, London, 2004).

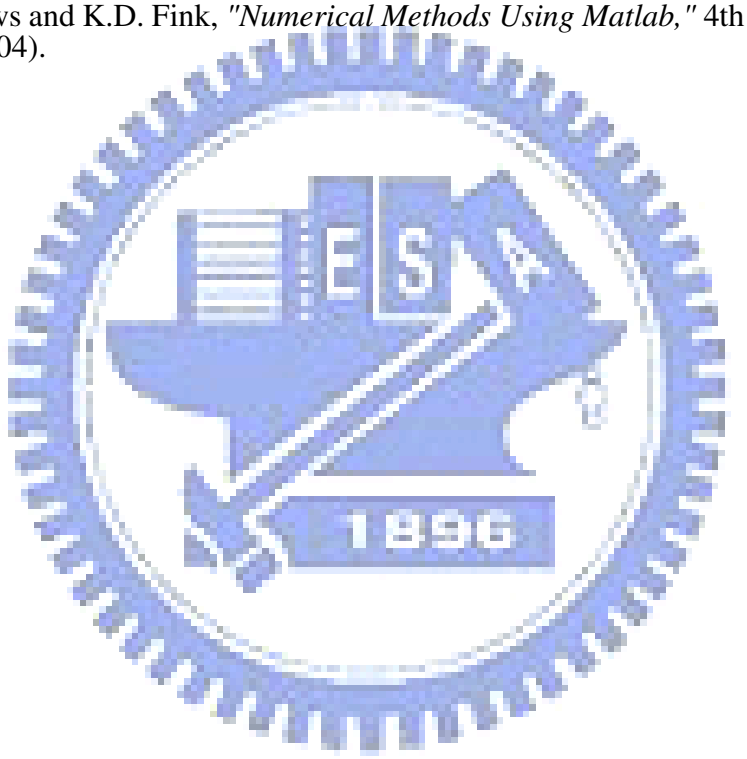

Appendix A The definition of weight factor in the wiggle-suppressing scheme

The wiggle-suppressing scheme to be abbreviated as w-α scheme. The extension is formed by Eq. (2.21) and

$$(u_{\overline{x}})_j^n = (\omega_-)_j^n \, (\widehat{u}_{\overline{x}+})_j^n + (\omega_+)_j^n \, (\widehat{u}_{\overline{x}-})_j^n \tag{A.1}$$

with

$$(\omega_\pm)_j^n = W_\pm \left((\widehat{u}_{\overline{x}-})_j^n , (\widehat{u}_{\overline{x}+})_j^n , \alpha \right) = \frac{\left| (\widehat{u}_{\overline{x}\mp})_j^n \right|^\alpha}{\left| (\widehat{u}_{\overline{x}-})_j^n \right|^\alpha + \left| (\widehat{u}_{\overline{x}+})_j^n \right|^\alpha}. \tag{A.2}$$

Because the scheme is an extension of the c-τ^* scheme in which $(u_{\overline{x}})_j^n$ is expressed as an weighted average of $(\widehat{u}_{\overline{x}-})_j^n$ and $(\widehat{u}_{\overline{x}+})_j^n$. In case that $\left| (\widehat{u}_{\overline{x}+})_j^n / (\widehat{u}_{\overline{x}-})_j^n \right|$ is very close to 1, the only way to prevent the weighted average from becoming almost a simple average is to increase the value of α used. However, this approach is impracticable because evaluation of x^α would be hamperd by very large round-off errors if α becomes very large. As such, there is a need to introduce new-weighted-averaging techniques that do not have the limitation discussed above. Two weighted-averaging formulae much more potent and flexible that discussed here were described briefly.

For motivation, note that Eqs. (A.1) and (A.2) can be expressed as

$$(u_{\overline{x}})_j^n = \omega_1 x_1 + \omega_2 x_2 \tag{A.3}$$

and

$$\omega_1 = \frac{s_1}{s_1 + s_2} \text{ and } \omega_2 = \frac{s_2}{s_1 + s_2} \; (s_1 + s_2 > 0) \tag{A.4}$$

respectively if

$$\begin{aligned} x_1 &\equiv (\widehat{u}_{\overline{x}-})_j^n \text{ and } x_2 \equiv (\widehat{u}_{\overline{x}+})_j^n \\ \omega_1 &\equiv (\omega_-)_j^n \text{ and } \omega_2 \equiv (\omega_+)_j^n \\ s_1 &\equiv \left|(\widehat{u}_{\overline{x}+})_j^n\right|^\alpha \text{ and } s_2 \equiv \left|(\widehat{u}_{\overline{x}-})_j^n\right|^\alpha \ (\alpha \geq 0) \end{aligned} \tag{A.5}$$

The derivation for the first scheme is derived as following. Let

$$\delta_\ell \equiv \omega_\ell - \frac{1}{2}, \ \ell = 1, 2. \tag{A.6}$$

Thus the set $\{\delta_\ell\}$, $\ell = 1, 2$ provides a measure of how far the weighted average is deviated from the simple average. In the following, a simple way to adjust this deviation will be introduced. Let

$$\delta_{\min} \equiv \min\{\delta_\ell\} \text{ and } \delta_{\max} \equiv \max\{\delta_\ell\}. \tag{A.7}$$

$$\sigma_{\max} \equiv \min\left\{\frac{1}{2\delta_{\max}}, -\frac{1}{2\delta_{\min}}\right\} > 1.$$

We can given any adjustable real parameter $\sigma > 0$, let

$$\delta_\ell^{'} \equiv \sigma\delta_\ell. \tag{A.8}$$

Then we define

$$\omega_\ell^{'} \equiv \frac{1}{2} + \delta_\ell^{'}. \tag{A.9}$$

, where

$$\sigma = \min\left\{\sigma_{\max}, \frac{\sigma_0}{|\nu|}\right\} \tag{A.10}$$

($\sigma_0 > 0$ is a preset parameter in the order on 1).

For the second scheme describe as follows. To proceed, the indices of s_ℓ, $\ell = 1, 2$, will be reshuffled such that

$$s_2 > s_1 > 0 \tag{A.11}$$

Let

$$\eta_1 \equiv \frac{s_2}{s_1} - 1. \tag{A.12}$$

Given any adjustable real parameter $\sigma > 0$, let (i) $\widetilde{s}_1 = s_1$ and $\widetilde{s}_2 = (1 + \sigma\eta_1)s_1$ and (ii)

$$\widetilde{\omega}_\ell \equiv \frac{\widetilde{s}_\ell}{\widetilde{S}},\ \ell = 1, 2. \tag{A.13}$$

where

$$\widetilde{S} \equiv \left(\sum_\ell \widetilde{s}_\ell\right) > 0. \tag{A.14}$$

Note that the current approach for amplifying the weight factors has one advantage over the approach described earlier, i.e., in the current approach, there is no upper bound for the value of σ one could use. Thus, in the current approach, Eq. (A.10) can be simplified as

$$\sigma = \frac{\sigma_0}{|\nu|} \tag{A.15}$$

where $\sigma_0 > 0$ again is a preset parameter in the order of 1.

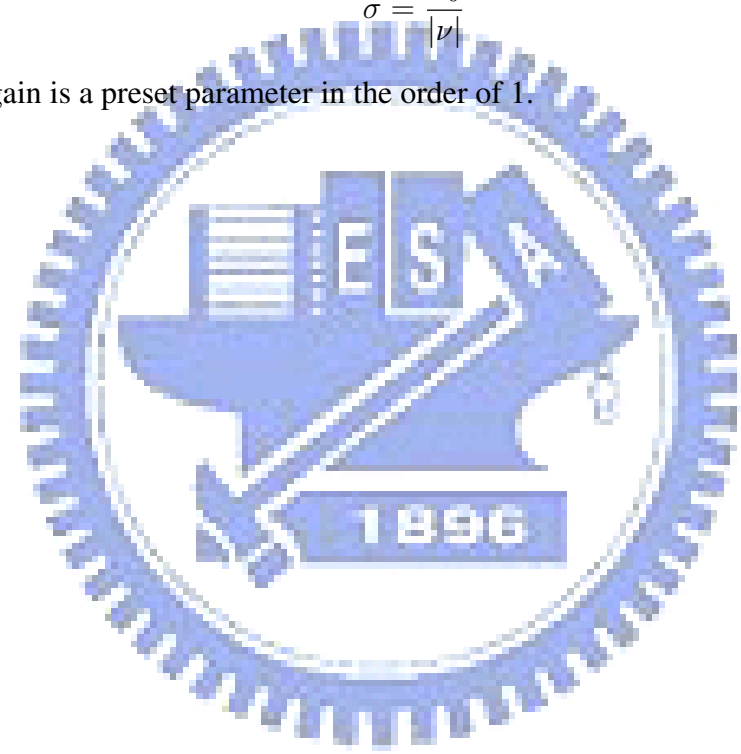

Vita

My name is Zhen-Ting Huang, aka Richard. I was born on November 11, 1984. I am currently studying in National Chiao Tung University. My major is Mathematical Modeling and Scientific Computing. My research area is atomic and molecule physics and other mathematical model simulation. I excel particularly in numerical analysis, large scale matrix computing, numerical optimization (linear programming), genetic algorithm, neural network and signal processing (wavelet analysis). I am experienced in parallel computing, three-dimension graph and grid generation. In addition, I am also familiar with several kinds of mathematical software including Matlab, Mathematical and Maple.